ESTCP Project No. 200105

UXO CHARACTERIZATION WITH A FAST 4-D TEM SYSTEM

PROGRESS REPORT(Revised): BLOSSOM POINT TESTS

April 27, 2002

Zonge Engineering and Research Organization
Tucson, AZ 85716

1. REPORT DATE **27 APR 2002**	2. REPORT TYPE	3. DATES COVERED **00-00-2002 to 00-00-2002**

4. TITLE AND SUBTITLE **UXO Characterization with a Fast 4-D Tem System**	5a. CONTRACT NUMBER
	5b. GRANT NUMBER
	5c. PROGRAM ELEMENT NUMBER
6. AUTHOR(S)	5d. PROJECT NUMBER
	5e. TASK NUMBER
	5f. WORK UNIT NUMBER
7. PERFORMING ORGANIZATION NAME(S) AND ADDRESS(ES) **Zonge Engineering and Research Organization,Tucson,AZ,85716**	8. PERFORMING ORGANIZATION REPORT NUMBER
9. SPONSORING/MONITORING AGENCY NAME(S) AND ADDRESS(ES)	10. SPONSOR/MONITOR'S ACRONYM(S)
	11. SPONSOR/MONITOR'S REPORT NUMBER(S)

12. DISTRIBUTION/AVAILABILITY STATEMENT
Approved for public release; distribution unlimited

13. SUPPLEMENTARY NOTES

14. ABSTRACT

15. SUBJECT TERMS

16. SECURITY CLASSIFICATION OF:			17. LIMITATION OF ABSTRACT	18. NUMBER OF PAGES	19a. NAME OF RESPONSIBLE PERSON
a. REPORT **unclassified**	b. ABSTRACT **unclassified**	c. THIS PAGE **unclassified**	**Same as Report (SAR)**	**44**	

INTRODUCTION

In accordance with our project plans, we conducted a demonstration of the Zonge 4-D NanoTEM system at the NRL Baseline Ordnance Classification Test Site located at the U.S. Army Research Laboratory's (ARL) Blossom Point facility[1]. Work was conducted at the facility during the period December 9-14, 2001 and generally followed the demonstration plan submitted to the ESTCP office in August, 2001 and approved with minor revisions in September, 2001[2]. The primary objective of the test was to demonstrate the "added value" of a multi-component TEM system with early time capability.

This progress report presents results from the demonstration and serves as a vehicle for the submission of a documented data set, an important deliverable that is part of our project plan. We submit herewith as Attachment A, a CD containing a large part of the data collected during the demonstration. Three data files in comma-separated-value (CSV) format include a) a data grid of the BP test area with north-south lines spaced at 0.5m, b) a similar grid with lines in the east-west direction at 1-m intervals, and c) a file containing all calibration repeat data. A PDF document describes the *Dynamic NanoTEM* (DNT) system used to acquire the data and serves as the data documentation.

The report also addresses an important *Action Item* communicated to us by ESTCP management and technical advisors. We have been asked to address the issue of comparative sensitivity between the Zonge NanoTEM system and the Geonics EM-61 and EM-63 instruments. Using data acquired at the Blossom Point UXO site and supplied to us by NRL, we present here a comparison of the sensitivity of the three systems.

DATA COLLECTION AND EXTENT

A map view of the main data grid acquired at Blossom Point is shown in Figure 1a. These data were compiled from a set of North-South lines spaced on ½ m intervals and a set of East-West lines spaced on 1-m intervals. The data were collected over a 2½ day period from December 11 through 13. When operating in its profile mode, the NanoTEM system samples the TEM transients at 31 time gates or windows that are centered at approximately uniform logarithmic time intervals after the transmitter current has been turned off. The system acquires and records data at a rate of 32 data points per second. The data shown in Figure 1 represent the station locations for data points collected. The high data rate causes the station locations to appear as continuous lines. The mapped area includes the 5 target columns (A-E) in the test area description[1]. An additional column (Z), located west of Column A, was installed subsequent to the referenced report.[1] Rows 1 through 12 of column Z are populated with 60mm mortar rounds at depths ranging from 25cm to 1m. The 1-m deep mortar targets are the only targets that were not detectable with the NanoTEM system.

Figure 1b is a color map compiled from the North-South data only. In Figure 1b, we have mapped a composite time gate representing *Comparison* time (21-213μs). The target columns (*Z, A-E*) and the target rows (*1-15*) are indicated for reference. The color scale on this map is logarithmic (10 intervals/decade) in an effort to provide an indication of the very large dynamic range of these data. With this color scale, some of the smaller targets (e.g., the 60mm mortars

---

[1] Two other columns (X, and Y) have been planted immediately west of Z. We have included data for Columns X and Y in our assessment in this report but were unable to include those data in the deliverable documented data set.

buried at 75cm at positions *Z-1*, *Z-2*, and *Z-3*) are barely discernable. However, most of these targets can be if we zoom in on a particular region of the map. We have dubbed the composite gate used for Figure 1b the ***Comparison*** gate since that is the time gate we have used in comparing sensitivities between the EM-61, EM-63, and NanoTEM systems. We caution the reader not to make qualitative comparisons between the various systems based on the quality of the color map presentations. Indeed, it is rather simple to grid the data

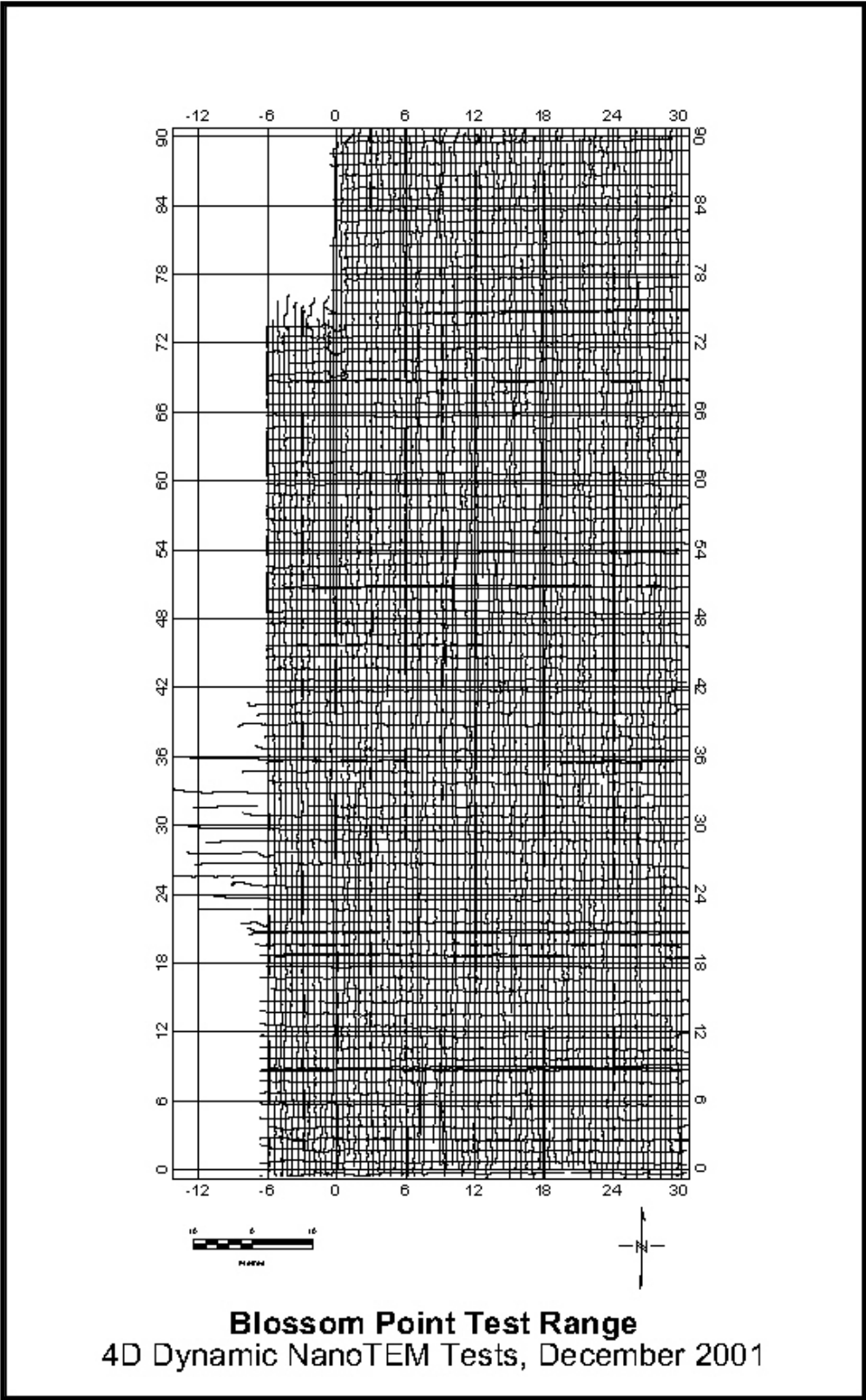**Blossom Point Test Range**
4D Dynamic NanoTEM Tests, December 2001

Figure 1a: DynanoTEM survey coverage at NRL's Blossom Point UXO test facility.
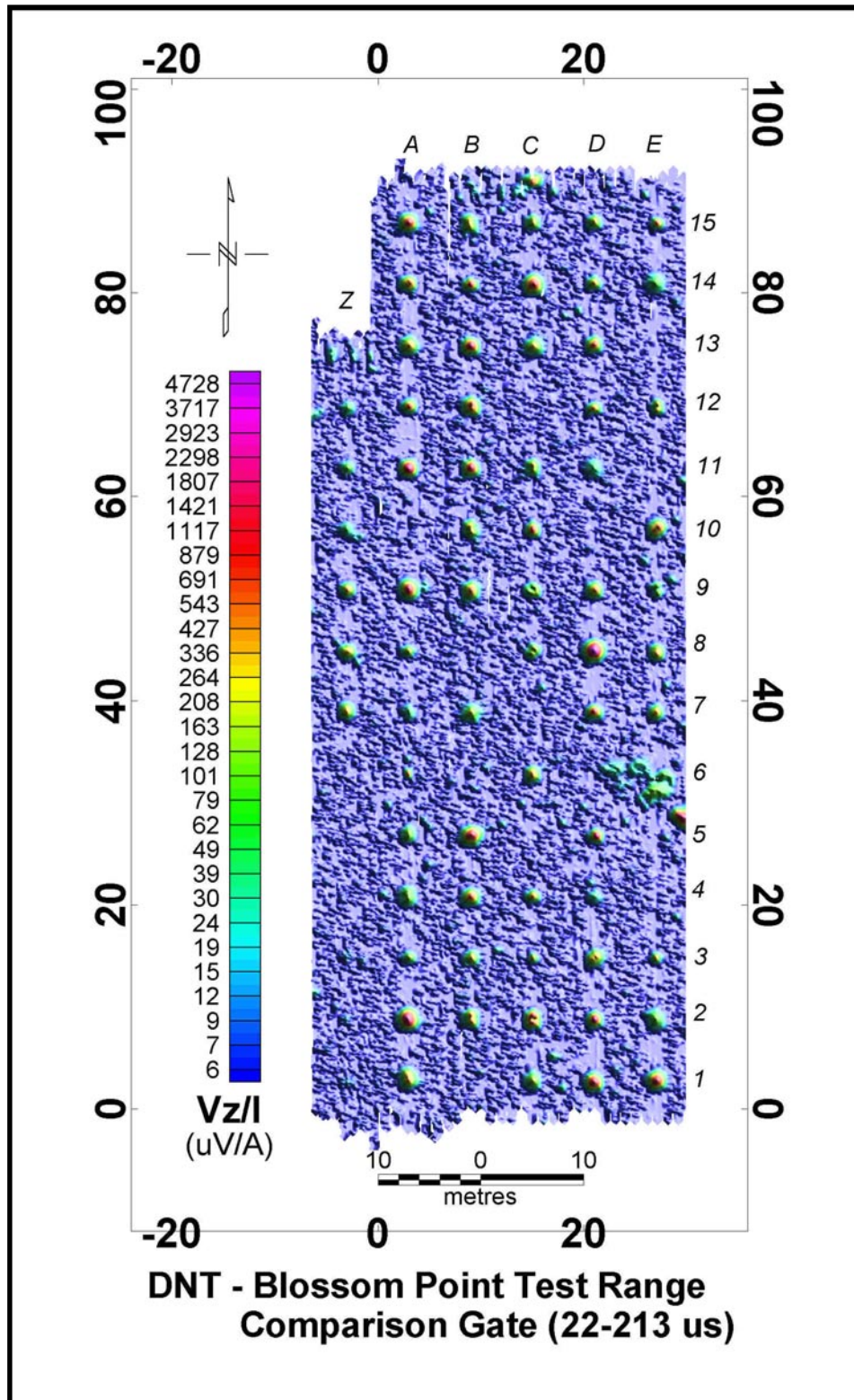
Figure 1b: Blossom Point Dynamic NanoTEM data. Vertical field, *Comparison* (22-213 μs) time gate.

Automatic Target Picking

We have prepared a "standard" color intensity map and target list to demonstrate that we have the tools to handle routine data. The map is shown in Figure 2 and a list of the targets that were picked automatically from this map is shown in Table 1.

The only manual editing applied to the data was splitting the original data into lines. Background was chosen and subtracted via an algorithm without manual intervention on any of the selected lines. The targets were selected with an algorithm and no targets have been added or eliminated from the list.

The starting point for this target selection exercise was raw transient data with corresponding coordinates, corrected for cart heading and offsets, and divided into lines. Background was automatically chosen along each profile. A background transient was fitted to the line and subtracted from each of the raw transients. Scalar data were extracted by summing windows 10 through 16, the so-called '*early*' window of the vertical, TEM_Z, component.[2] These data were filtered with a 25-point low-pass filter. The result was companded using the function ArcSinh(data/25).[3] These data were gridded using a Minimum Curvature gridding routine. The grid was contoured and plotted. Targets were chosen using a Blakely Test picking algorithm after 12 passes with a smoothing filter and using a cutoff value of 0.2. We have displayed the results as a color image with the target picks marked with posted '+' symbols in Figure 2.

The resulting list of targets was examined and scored. The known targets were identified. Then targets very near the edge of the grid were marked as "out of bounds." The rest of the targets were marked as false alarms. Field notes were examined and an attempt was made to correlate some of the false alarms to known items in the field such as a hammer used to drive stakes and the metal "swivels" at the end of the survey we used as lane markers. Correlations are noted.

Four targets were missed. One is target X-5S, a 30 mm shell, 2 cm deep, in the south half of cell X-5. The anomaly from this target is apparent in the data. It can be detected by adjusting the sensitivity of the picking algorithm. Of course this would also cause more false alarms. The three 1-m deep mortars are not detectable with this system.

In this exercise, we detected 78 of 82 targets with 31 False Alarms, 23 detections on the fringe of the grid, and 11 noted items of surface clutter. Of the 31 False Alarms, 2 anomalies (ID Nos. 103 and 97) are almost certainly due to items left on the parameter of the field survey. These anomalies occur at X = 29.6 m and 29.8 m, within a few inches of the eastern boundary of the surveyed area.

---

[2] Our experience with the DNT system is limited at this point to the Blossom Point data set. Based on these data, it appears that for the purpose of automatically detecting anomalies based on some threshold, some measure of the vertical response is arguably the best parameter to use. However, as we mention farther along in the report, the amplitude of the horizontal field as calculated in some composite time gate also generates an anomaly that is centered over the target. The maps of this parameter look very much like a vertical component map. Under some circumstances, therefore, it may be that targets of interest can be picked more reliably from a horizontal field amplitude map.

[3] The companding function ArcSinh() provides a near logarithmic compression of high-level signals of either polarity and a more linear response at low levels. The normalization factor (25 µV/A in this case) indicates the threshold above which the function acts more like a logarithm.

Table 1: Target list generated with automatic detection

X	Y	Grid value	Mask	Target ID	Interpretation
15.2	91	1.5	1	144	Hammer?[4]
22.6	90.6	0.2	1	143	Out of bounds
17.2	90.2	0.3	1	142	Out of bounds
9.6	90	0.2	1	141	Out of bounds
7	89.8	0.4	1	140	Out of bounds
26	89.6	0.3	1	139	Out of bounds
5	88	0.4	1	138	Swivel
-0.4	87.4	0.2	1	137	Out of bounds
27.2	86.8	1.6	1	136	E-15
21	86.8	1.2	1	135	D-15
15.2	86.8	1.1	1	134	C-15
9	86.8	1.3	1	133	B-15
3	86.8	1.9	1	132	A-15
0.6	85	0.2	1	131	False Alarm
29.8	81.8	0.2	1	130	Out of Bounds
27	80.8	0.7	1	129	E-14
21	80.8	1.3	1	128	D-14
15.2	80.8	1.8	1	127	C-14
9	80.8	1.9	1	126	B-14
3	80.8	1.6	1	125	A-14
19.4	78.2	0.4	1	124	False Alarm
21	74.8	1.6	1	123	D-13
15.2	74.8	1.2	1	122	C-13
9	74.8	2	1	121	B-13
3	74.8	1.3	1	120	A-13
0	74.6	1	1	119	Out of Bounds
-4.4	74.2	0.4	1	118	Out of Bounds
-0.4	72.6	0.3	1	117	Out of Bounds
30.6	69	0.9	1	116	Hammer?
27.2	68.8	1.1	1	115	E-12
9.2	68.8	1.6	1	114	B-12
3	68.8	1.7	1	113	A-12
21	68.6	1.4	1	112	D-12
-3	68.6	0.6	1	111	Z-12
-5.8	68.2	0.4	1	110	Swivel
10.8	67.2	0.2	1	109	False Alarm
21	62.8	0.6	1	108	D-11
15	62.8	1.3	1	107	C-11
9	62.8	2	1	106	B-11

---

[4] The north end of the NS grid was at y=90m for $0 \le x \le 30m$. We sometime left a hammer at the end of the lane markers. The anomalies marked "hammer" are in fact out-of-bounds.

X	Y	Grid value	Mask	Target ID	Interpretation
3	62.8	2.1	1	105	A-11
-3	62.8	0.8	1	104	Z-11
29.6	61.6	0.4	1	103	False Alarm
30.2	58	0.2	1	102	Out of bounds
27.2	56.8	1.6	1	101	E-10
15	56.8	1.8	1	100	C-10
9	56.8	1.3	1	99	B-10
-3	56.8	0.7	1	98	Z-10
29.8	54	0.3	1	97	False Alarm
26	53.8	0.3	1	96	False Alarm
28.6	51.8	0.5	1	95	False Alarm
27.2	50.8	0.6	1	94	E-9
21.2	50.8	1.5	1	93	D-9
15	50.8	0.9	1	92	C-9
9	50.8	1.5	1	91	B-9
3	50.8	2	1	90	A-9
-3	50.8	1.4	1	89	Z-9
-5.8	48.8	0.2	1	88	Out of bounds
7.6	48.2	0.2	1	87	False Alarm
-6.8	45.6	0.2	1	86	Out of bounds
21	44.8	2.5	1	85	D-8
15	44.8	1.1	1	84	C-8
3	44.8	1.3	1	83	A-8
-3	44.8	1.4	1	82	Z-8
27.2	44.6	1.4	1	81	E-8
28	41.4	0.4	1	80	False Alarm
15.8	41.2	0.3	1	79	False Alarm
30.4	39.8	0.2	1	78	Out of bounds
-3	39	1.4	1	77	Z-7
27	38.8	1.4	1	76	E07
21	38.8	1.8	1	75	D-7
9.2	38.8	1	1	74	B-7
3	38.8	0.6	1	73	A-7
-12	38.4	0.3	1	72	False Alarm
-13.4	37.8	0.6	1	71	False Alarm
30	37.6	0.5	1	70	Out of bounds
28.2	36.2	0.2	1	69	False Alarm
-11.8	36	0.2	1	68	X-6N
-9	35.8	1.2	1	67	Y-6N
25.4	33.6	0.5	1	66	False Alarm
23.2	33.4	0.5	1	65	False Alarm
15	32.8	1.4	1	64	C-6

X	Y	Grid_value	Mask	Target_ID	Interpretation
3	32.8	1.7	1	63	A-6
-9	32.8	0.5	1	62	Y-6S
-12	32.8	1.1	1	61	X-6S
30.8	31.6	0.6	1	60	Out of bounds
9.4	31.4	0.4	1	59	False Alarm
27	31.2	0.9	1	58	False Alarm
-5.2	31	0.2	1	57	False Alarm
-10.2	31	0.2	1	56	False Alarm
16.4	30	0.2	1	55	False Alarm
14	30	0.3	1	54	Swivel
6.8	29.8	0.2	1	53	Swivel
1.2	29.8	0.2	1	52	Swivel
-9	29.8	1.1	1	51	Y-5N
-12	29.8	0.2	1	50	X-5N
20	29.6	0.3	1	49	Swivel
29.8	28.6	2.3	1	48	Hammer?
4.2	28.4	0.3	1	47	False Alarm
24	28.2	0.4	1	46	Swivel
18	28.2	0.4	1	45	Swivel
12	28	0.3	1	44	Swivel
21.2	26.8	2.1	1	43	D-5
9	26.8	2	1	42	B-5
3	26.8	1	1	41	A-5
-12	26.8	0.5	1	40	X-5S
28	26.4	0.3	1	39	False Alarm
15.2	25.2	0.3	1	38	False Alarm
5	24	0.3	1	37	False Alarm
-9	23.8	0.8	1	36	Y-4N
30	23.4	0.2	1	35	Out of bounds
0.8	21	0.3	1	34	False Alarm
21	20.8	0.5	1	33	D-4
15	20.8	1.4	1	32	C-4
9	20.8	1.7	1	31	B-4
3	20.8	1	1	30	A-4
-6	19.6	0.3	1	29	Out of bounds
29.2	19	0.2	1	28	False Alarm
11.8	15.6	0.5	1	27	False Alarm
-3	15	0.2	1	26	Z-3
27	14.8	1.3	1	25	E-3
21.2	14.8	1.4	1	24	D-3
15	14.8	1.1	1	23	C-3
9.2	14.8	1.3	1	22	B-3
3	14.8	0.9	1	21	A-3

| X	Y	Grid value	Mask	Target ID	Interpretation
30.4	12	0.3	1	20	Out of bounds
-6	11.4	0.3	1	19	Out of bounds
27	8.8	0.9	1	18	E-2
21	8.8	2.1	1	17	D-2
15	8.8	1.4	1	16	C-2
9.2	8.8	1.5	1	15	B-2
3	8.8	2.2	1	14	A-2
-3	8.8	0.2	1	13	Z-2
30.4	7.6	0.4	1	12	Out of bounds
3.6	5.4	0.2	1	11	False Alarm
17.2	5.2	0.6	1	10	False Alarm
30.6	3.8	0.3	1	9	Out of bounds
23.4	3.8	0.2	1	8	False Alarm
3	3	1.5	1	7	A-1
27.2	2.8	2	1	6	E-1
15	2.8	1.1	1	5	C-1
21	2.6	2	1	4	D-1
-2.8	2.6	0.2	1	3	Z-1
18	2.2	0.6	1	2	False Alarm
8.8	-0.2	0.3	1	1	Out of bounds
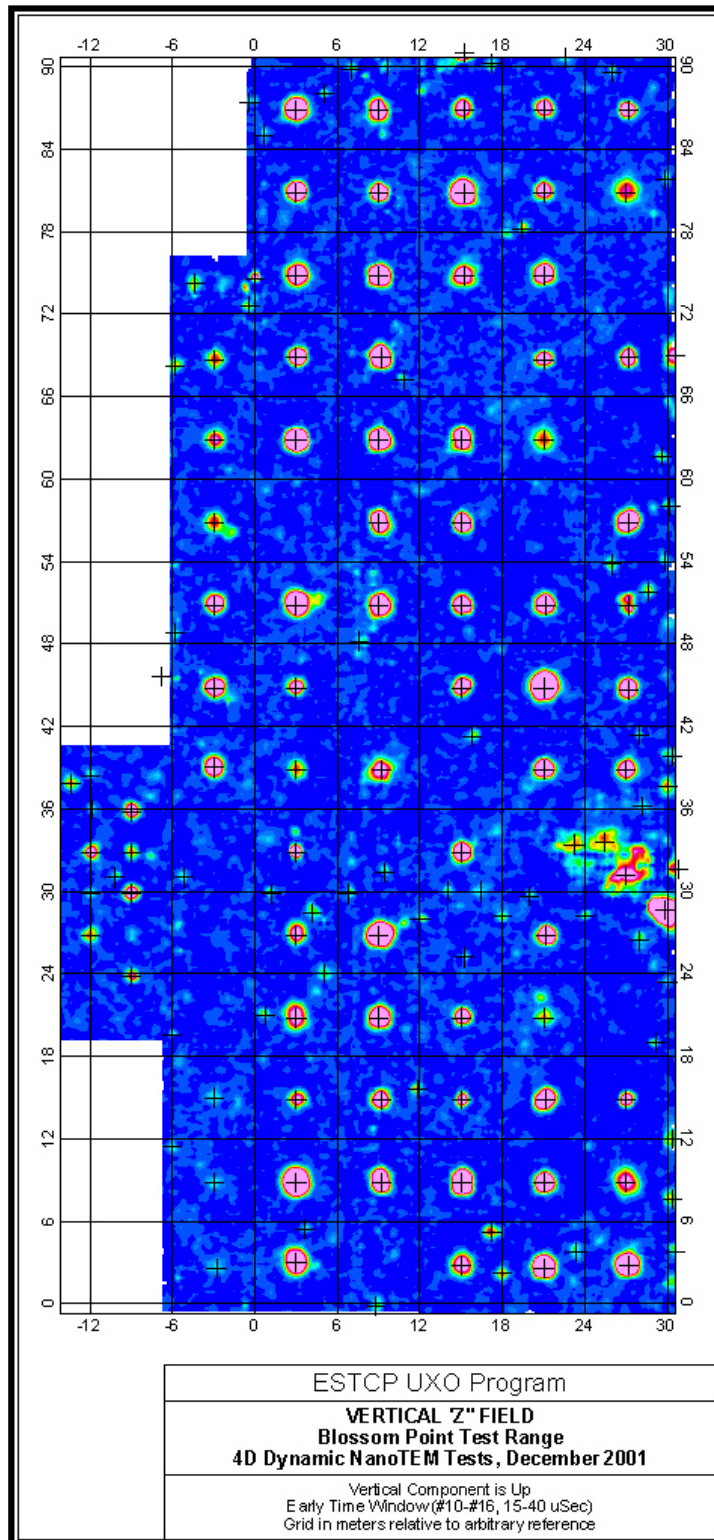
Figure 2: Standard map of the *Early* time vertical field intensity used for automatic anomaly picking.

COMPARATIVE RESPONSE

There is considerable interest in the UXO community in the comparative sensitivity between various systems. At the specific request of ESTCP management, we have been given as an *Action Item* the task of comparing our NanoTEM system with both the EM-61 and the EM-63. We used data sets supplied to us by NRL (BPEM63unlev.csv – EM-63, and BPNorthSouth.txt – MTADS Man-Portable EM-61). As implied by the EM63 file name, those data were unleveled. After subjected these data sets to a line-by-line background removal, these data sets are displayed as color-shaded intensity maps in Figures 3 and 4. The data sets for these maps have therefore undergone the exact same processing and are displayed with the same display parameters as the DNT data shown in Figure 1b. We offer these three color displays for qualitative comparison with only one comment. It would appear that for the time gates compared, the EM-61 has a larger dynamic range over the Blossom Point test objects than either the EM-63 or the NanoTEM systems.

Comparison Methodology

Quantitative comparisons between the three data sets were affected by measuring the ratio of the peak response of each of the anomalies in Columns Z, and A-E to an estimate of the average background noise level for the respective data sets. Anomaly statistics are easily determined within the Geosoft Oasis Montaj software package. Background was removed for each system. The noise value taken for each system significantly affects the comparative results. Anomaly peaks were picked using appropriate centerline profiles. Depending on the amount of low-pass filtering that we apply to the DNT data, we can change the noise value of our system. The noise value for the NanoTEM system was based on filtering the profile data with a 1-sec low-pass filter. For the record, we used the following noise values in computing signal-to-noise ratios (SNR) for the systems under study:

Table 2: Noise figures used for system comparisons

System	Noise Value
EM-61	5 mv
EM-63	1.3 mv
NanoTEM	6 μv

The SNR for each of the targets expressed in decibels (dB) is tabulated in Table 3. Signal levels for both Geonics systems are based on the reported voltage measured at the lower coil. In the case of the EM-63, the signal was measured on the composite gate formed by summing gates 2 through 10. In the NanoTEM system, we summed gates 12 through 21 resulting in a time window of 21.7μs to 213.3μs. As we mentioned previously, this gate was chosen arbitrarily as the *Comparison* time gate.

Comparing the sensitivity of the NanoTEM system with the EM-61 is straightforward since the standard EM-61 measures a single component of the TEM transient over a well-defined time interval.[5] Comparisons between the EM-63 and the NanoTEM system are more difficult since each has multiple time gates. We compared the two systems by choosing a composite window

---

[5] The standard EM-61 time gate is defined as the interval (370μs, 870μs)

(2 through 10)[6] for the EM-63 (bottom coil). We did a small amount of experimenting with EM-63 composite gates in order to choose a window that, qualitatively at least, made the best map. However, we did not attempt to determine the "optimum" composite gate for the Blossom Point target set. The comparative SNR's between the NanoTEM system and the EM-63 depends on the selection of time gates. So while we believe this comparison provides a reasonable semi-quantitative measure of relative sensitivity, the comparison can be modified by selecting a different gate for either system and by changing the filtering parameters in the NanoTEM system. We concede here that it would be unfair of us to conclude from this comparison that NanoTEM is necessarily more sensitive than the EM-63. But we do conclude that our system has a sensitivity that is comparable to its competitors.

---

[6] We have been unable to obtain the exact window widths and times for the EM-63 at the writing of this report.
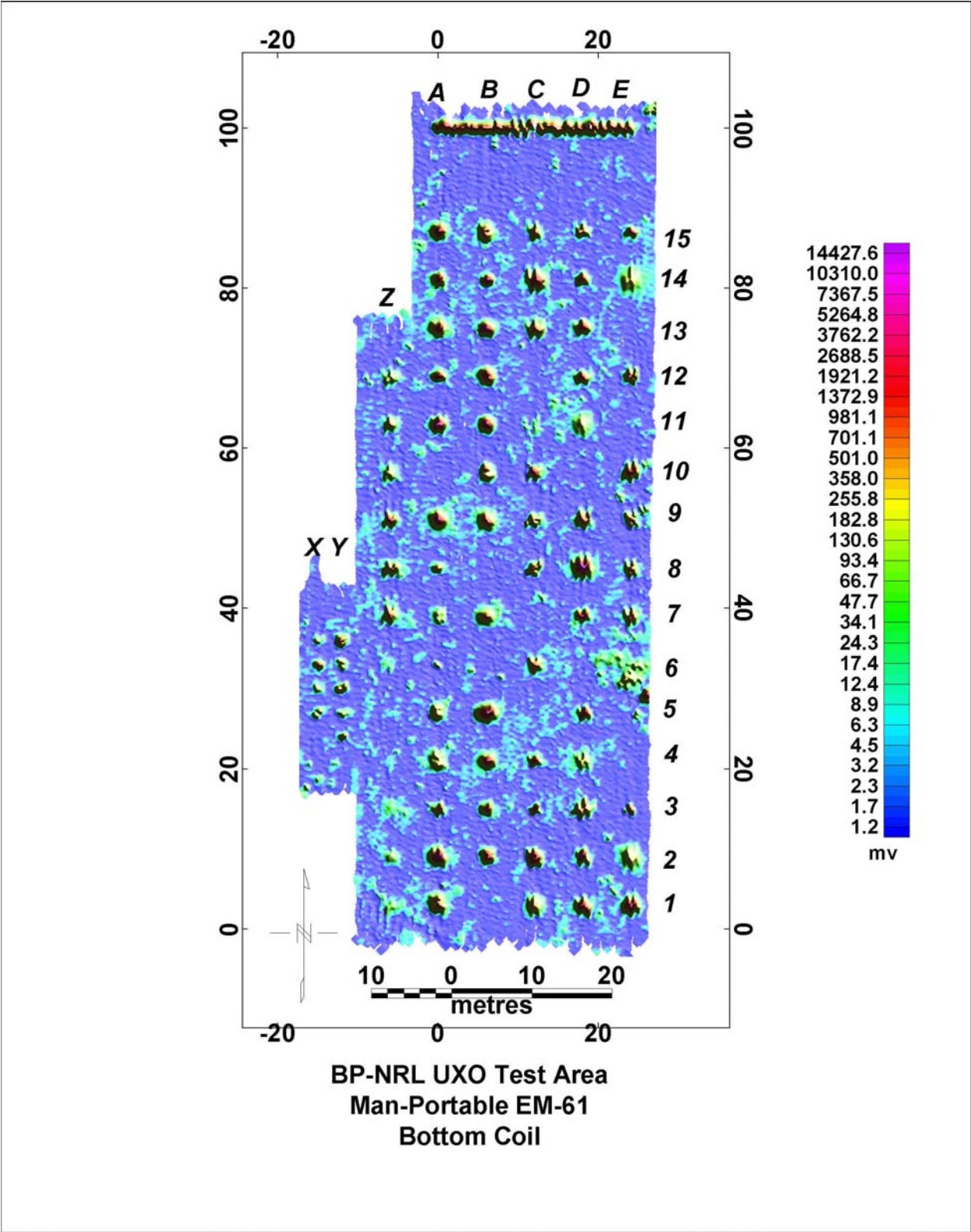
Figure 3: Man-portable MTADS data set for Blossom Point comparison.
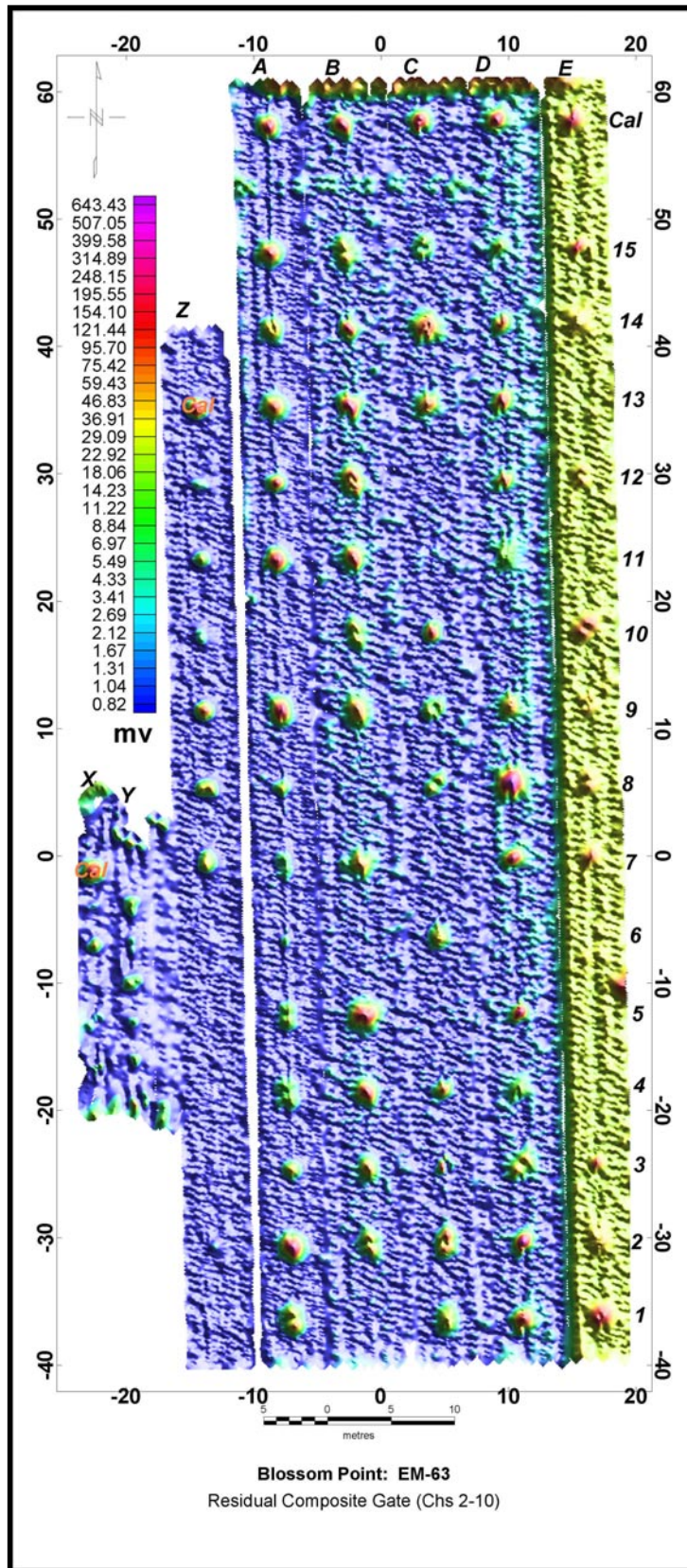
Figure 4: EM-63 data set for Blossom Point – Lower Coil (Composite Gate 2-10)

Using the SNR's presented in Table 3, we have computed a relative signal amplitude (expressed in decibels) between the three systems with the NanoTEM system used as a reference. These results are presented in Table 4. From that table, we see that, in general, the EM-61 is slightly more sensitive than the NanoTEM system while the EM-63 is uniformly less sensitive (with the caveat that these results may change either way by comparing different response parameters and by post-acquisition filtering).
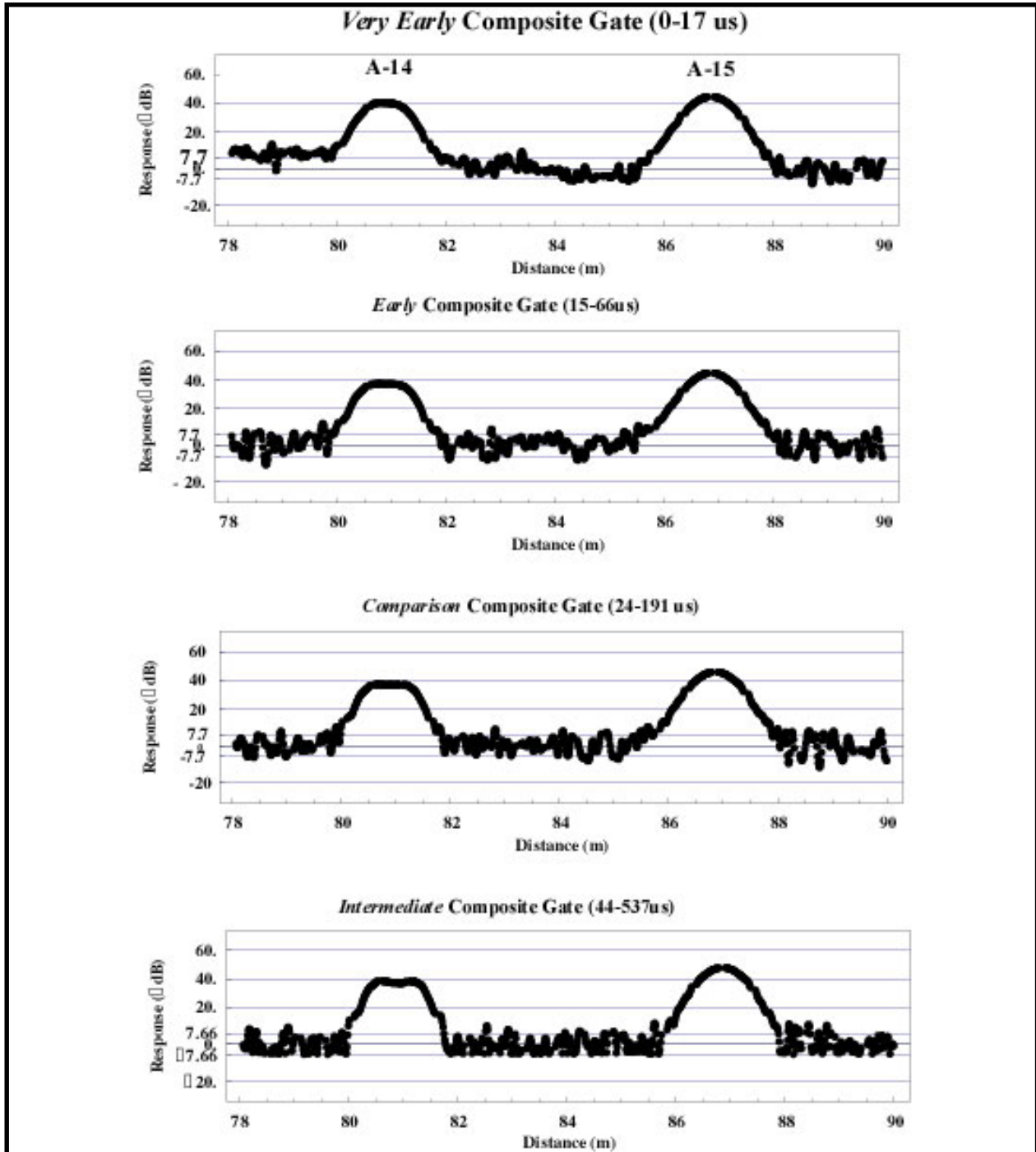

Figure 5a: Comparison of target response for 4 different composite time gates for the NanoTEM system. The *Comparison* gate is the gate we compared with the EM-61 and EM-63.

We have experimented a little with finding an optimum gate for detection. In Figure 5a we show a section of the NS centerline profile along Column A that includes targets A-14 and A-15, left to right. These targets are, respectively, a 4"x4"x1/4" steel plate, and 16 lb shotput. These curves are plotted here with only minimal low-pass filtering (4 Hz low-pass) in order to provide a sense of the intrinsic noise. We remind the reader that the comparison was made from centerline profiles filtered with a 1 Hz LP filter. Note also, that these curves have been plotted with a companding function, with each curve normalized to an estimate of the mean deviation in the corresponding gate background as measured between 82.5m and 85.5m. In these plots, the amplitudes are approximately linear between –7.7 and 7.7 and they are approximately logarithmic at amplitudes greater than 7.7. The amplitudes at the anomaly peaks therefore represent a good estimate of the signal-to-noise (SNR). For example, the peak amplitude of anomaly A-15 in the *Comparison* gate (3rd curve in Figure 5a is approximately 45-50 dB. This agrees with the 54.4 reported in Table 3. Additional LP filtering dramatically reduces the noise as illustrated in Figure 5b. Here we compare the *EM-61* composite gate with minimal (4 Hz LP filtering) to the same profile segment after filtering with a 1 Hz LP filter.
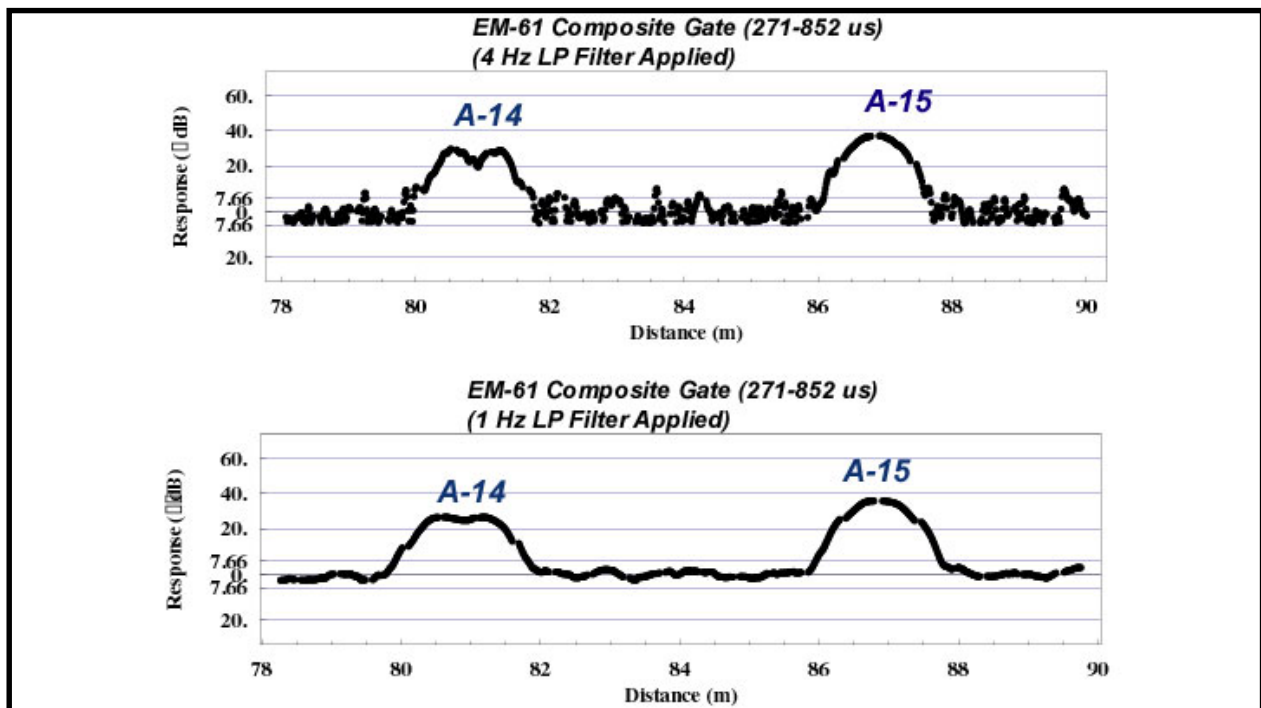

Figure 5b: The effect of low-pass filtering for noise reduction.

The *Intermediate* composite time gate (bottom curve) consisting of NanoTEM gates 15-25 (43.5 to 537.4 μs) has the best SNR of the 4 gates shown. The gate in Figure 5b is close to an EM-61 (i.e., ~500 μs wide starting at about 300 μs). The two anomalies plotted using either the *Comparison* or *Intermediate* composite gates have a significantly greater SNR than the anomalies plotted using the *EM-61* gate. Moreover, the *Intermediate* is marginally better than the *Comparison* gate. However, the anisotropic polarization behavior (as evidenced by the double peaked behavior) of the plate anomaly on the left is better developed in the gates with later times (i.e., *Intermediate* and *EM-61*). We believe this observation has important

ramifications when applying inversion methods to full transient waveforms and no doubt also to broadband spectra from frequency domain instruments.

Of course, optimum gates depend on target populations. With close examination of the target anomaly population at Blossom Point, we can see variation in the amplitudes of the anomalies relative to the gate used to plot them that is inconsistent with the inference from Figure 5 that a particular time gate is somehow has a uniformly better SNR by a simple multiplicative constant factor (e.g., the *Intermediate* gate has 5dB better SNR). This is because these anomalies have different broadband responses. Because of its early time response characteristics, the NanoTEM system responds well to small targets and, as such, the 12-21 gate that we used in the comparisons for Table 3 show significantly higher NT responses for some conductive targets (e.g., target A-6, a flattened aluminum pop can).

Figure 5 illustrates an instrumental problem that requires some work. The very early time window exhibits a variation in the background that is not seen in the later time gates. We believe that this background variation is caused by some instability in our transmitter turn-off ramp.[7] It represents a limitation to early times in the vertical channel. In general, we have noted that the earlier time windows almost always give signal-to-noise responses that are as good or better than later time windows but this is compromised by this instrumental drift, especially for the vertical component. For this reason, we have used our *very early time window* (0 to 15 μs) for the horizontal components and our *early time window* (15 to 40 μs) for the vertical component in figures.

---

[7] We are studying this early time background drift. We believe it is caused by temperature variations in the fly-back diodes that are used to protect our solid state switching devices. We are currently searching for faster and more stable diodes. We believe improvements in the transmitter will result in very usable results at *very early* times in the vertical field as well as in the horizontal field.

Table 3 Signal-to-noise comparison (expressed in dB) between the EM-61, EM-63 (chs 2-10), and NanoTEM (chs 12-21)/

	Z			A			B			C			D			E			
	EM-61	EM-63	NT	EM-61	EM-63	NT	EM-61	EM-63	NT	EM-61	EM-63	NT	EM-61	EM-63	NT	EM-61	EM-63	NT	
15				55.5	40.1	54.4	48.1	31.2	41.4	41.2	26.3	38.9	37.4	26.6	41.6	50.8	42.9	51.4	15
14				47.9	30.1	46.3	57.5	44.6	54.2	52.3	36.9	51.2	49.3	37.5	44.5	31.9	30.3	32.5	14
13				49.6	38.2	44.4	61.4	46.8	58.0	44.8	36.2	42.1	42.3	41.1	50.6	NT	NT	NT	13
12	30.6	18.2	28.4	53.0	42.6	52.7	53.7	38.2	48.4	NT	NT	NT	39.1	36.5	45.9	45.8	33.4	41.1	12
11	39.1	27.5	33.8	55.0	43.3	59.9	52.4	40.4	55.4	20.5	NA	40.1	26.5	20.3	29.0	NT	NT	NT	11
10	30.2	19.0	29.2	NT	NT	NT	39.4	29.9	40.1	52.2	41.5	52.2	NT	NT	NT	40.9	36.8	49.1	10
9	47.8	37.6	46.0	59.8	45.8	57.4	46.9	34.9	46.5	39.1	24.2	35.2	45.1	33.1	46.5	45.3	31.9	39.1	9
8	43.9	29.9	43.5	42.4	28.3	41.9	NT	NT	NT	41.7	25.0	36.3	69.0	41.9	67.7	47.5	33.8	45.7	8
7	41.0	30.6	43.1	28.9	20.3	28.2	40.8	33.7	38.0	NT	NT	NT	49.5	47.0	55.3	48.0	36.8	46.1	7
6	NA	NA	NA	25.7	19.7	49.8	NT	NT	NT	48.1	31.2	44.1	NT	NT	NT	NT	NT	NT	6
5	NA	NA	NA	35.7	25.4	35.3	58.0	43.2	55.3	NT	NT	NT	41.2	46.7	59.2	NT	NT	NT	5
4	NA	NA	NA	37.0	23.8	35.5	56.3	42.6	36.6	48.1	36.9	45.5	31.9	23.8	28.2	NT	NT	NT	4
3	15.8	11.4	18.4	41.1	31.2	36.3	43.7	33.5	41.7	46.5	34.7	40.6	45.7	28.8	42.2	49.6	38.4	44.8	3
2	15.8	15.5	18.1	61.8	48.6	60.9	53.0	32.8	45.3	56.7	39.0	52.4	62.9	51.5	60.3	36.0	30.5	34.4	2
1	22.4	11.4	19.4	46.6	33.8	44.7	NT	NT	NT	41.1	27.8	37.6	53.3	40.4	55.8	51.9	40.4	55.4	1
	Z			A			B			C			D			E			

NT = No target present

NA = No anomaly detected

Table 4: Target amplitude relative to NanoTEM response (see Table 3). The numbers are in decibels relative to the SNR of corresponding peak NanoTEM response.

	Z			A			B			C			D			E			
	EM-61	EM-63	NT	EM-61	EM-63	NT	EM-61	EM-63	NT	EM-61	EM-63	NT	EM-61	EM-63	NT	EM-61	EM-63	NT	
15				1.0	(14.4)	0.0	6.6	(10.2)	0.0	2.4	(12.5)	0.0	(4.2)	(14.9)	0.0	(0.6)	(8.5)	0.0	15
14				1.7	(16.2)	0.0	3.3	(9.5)	0.0	1.1	(14.4)	0.0	4.8	(7.0)	0.0	(0.7)	(2.3)	0.0	14
13				5.2	(6.2)	0.0	3.5	(11.2)	0.0	2.7	(5.9)	0.0	(8.3)	(9.5)	0.0	NT	NT	NT	13
12	2.2	(10.2)	0.0	0.3	(10.1)	0.0	5.2	(10.2)	0.0	NT	NT	NT	(6.8)	(9.4)	0.0	4.6	(7.7)	0.0	12
11	5.3	(6.3)	0.0	(4.8)	(16.5)	0.0	(3.1)	(15.1)	0.0	(19.6)	NA	0.0	(2.5)	(8.7)	0.0	NT	NT	NT	11
10	1.0	(10.2)	0.0	NT	NT	NT	(0.8)	(10.3)	0.0	(0.1)	(10.8)	0.0	NT	NT	NT	(8.2)	(12.3)	0.0	10
9	1.8	(8.4)	0.0	2.4	(11.6)	0.0	0.4	(11.6)	0.0	3.9	(11.0)	0.0	(1.4)	(13.4)	0.0	6.2	(7.2)	0.0	9
8	0.4	(13.6)	0.0	0.5	(13.6)	0.0	NT	NT	NT	5.4	(11.3)	0.0	1.3	(25.8)	0.0	1.8	(11.9)	0.0	8
7	(2.1)	(12.4)	0.0	0.7	(7.9)	0.0	2.8	(4.3)	0.0	NT	NT	NT	(5.8)	(8.3)	0.0	2.0	(9.3)	0.0	7
6	13.1	NA	NA	(24.2)	(30.1)	0.0	39.0	NT	NT	3.9	(12.9)	0.0	NT	NT	NT	0.2	NT	0.0	6
5	NA	NA	NA	0.4	(9.9)	0.0	2.7	(12.1)	0.0	NT	NT	NT	(18.0)	(12.5)	0.0	126.0	NT	NT	5
4	NA	NA	NA	1.5	(11.6)	0.0	19.7	6.0	0.0	2.6	(8.6)	0.0	3.7	(4.3)	0.0	NT	NT	NT	4
3	(2.6)	(7.0)	0.0	4.8	(5.1)	0.0	2.0	(8.2)	0.0	5.8	(6.0)	0.0	3.5	(13.5)	0.0	4.8	(6.4)	0.0	3
2	(2.2)	(2.6)	0.0	0.9	(12.3)	0.0	7.7	(12.5)	0.0	4.3	(13.4)	0.0	2.7	(8.7)	0.0	1.6	(4.0)	0.0	2
1	3.0	(8.0)	0.0	1.9	(10.9)	0.0	NT	NT	NT	3.5	(9.9)	0.0	(2.6)	(15.4)	0.0	(3.5)	(15.0)	0.0	1
	Z			A			B			C			D			E			

NT = No Target present
NA = No Anomaly detected

HORIZONTAL COMPONENTS

The 4-D NanoTEM system samples 31 time gates along the transients from 3 orthogonal receivers. Figure 6 shows centerline profiles of the 3 components along column A. These data have been very lightly filtered (1/4s low-pass) in order to illustrate the larger noise levels present in the horizontal components, particularly in the later time windows.[8] Average noise levels are shown for each component. Note that the noise level in the H_x (along profile) component is nearly 10 times higher than in H_z and 5 times higher than for H_y. Fortunately, the noise is random and approximately gaussian and, therefore, we can reduce it by the application of a simple low-pass filter. A one second low-pass filter (i.e., 32 point wavelengths) still preserves the fidelity of the curve shape while reducing the noise by a factor of 3 as illustrated in Figure 7.
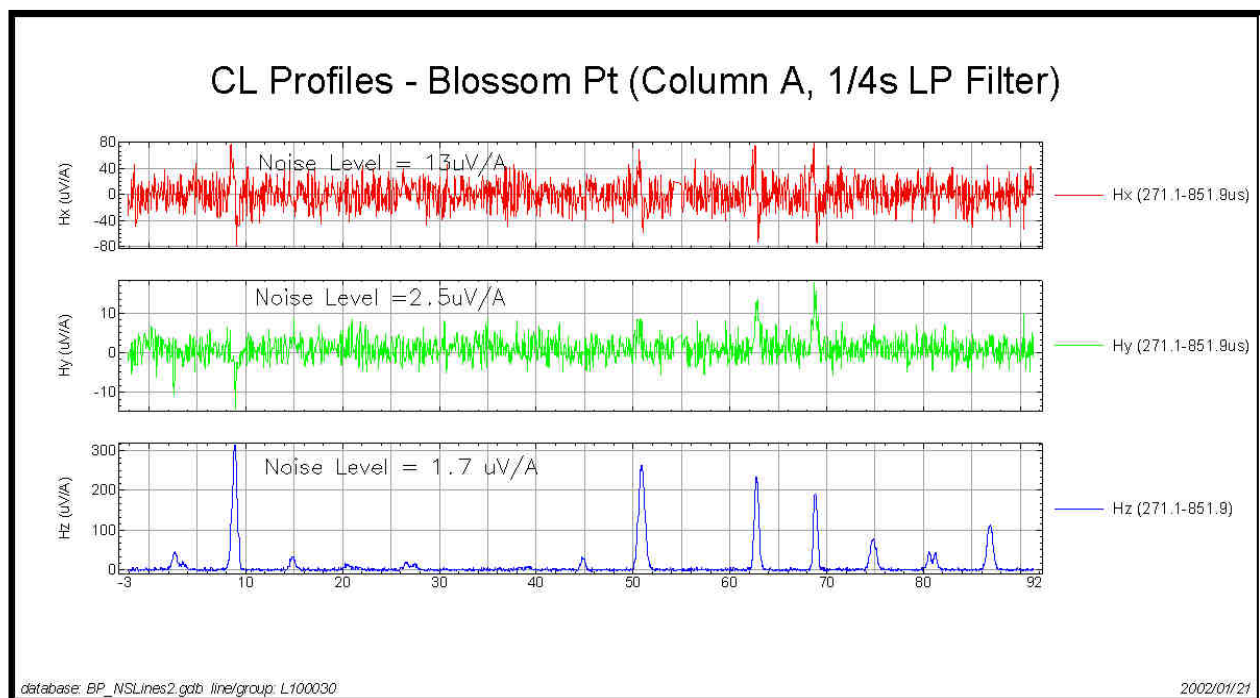
Figure 6: **Minimally filtered orthogonal components for a center-line Profile along Column A. The figure indicates noise levels. The time gate shown is our *EM-61* equivalent time gate.**

Zonge has evidence from other deployments of this system that suggests the horizontal components, particularly at early times, can detect the presence of a target object before the vertical component[3]. However, at Blossom Point we do not see any evidence of this capability. We speculate that because most of the targets are relatively shallow, conductive and magnetically permeable they are always well expressed in the vertical field component. The horizontal components have considerably higher noise levels than the vertical components,

---

[8] We believe the higher noise levels in the horizontal components are caused by high-frequency electromagnetic interference in the AM band. Horizontal magnetic fields do not couple well into the earth and hence are not attenuated as much as the vertical magnetic fields that are maximally coupled with the earth. In Figure 6, the noise in Hx is noticeably greater than in Hy. This suggests that the source of the noise at Blossom Point comes mainly from North or South of the ARL site.

particularly at late times. Generally speaking, the vertical component is visible as soon as and sometimes before the horizontal components begin to "pop" out of the noise background.

A profile plot showing *Very Early Time* (0-13μs) NanoTEM response for the two horizontal components together with the corresponding later time responses for the vertical component is presented in Figure 8. The horizontal component anomalies are more evident and coherent at early times than they are at late times. Horizontal component anomalies are bipolar features with a zero-crossing directly over the target. The anomaly's positive peak is positive when the measuring point has a positive offset with respect to the target along a particular horizontal axis.

The profile in Figure 8 was acquired while the cart was traveling south, so in the cart coordinate system positive *x* is south and positive *y* is east. The H_y profile (center profile in Figure 8) suggests therefore that our profile passed somewhat east (left) of targets A-10 through A-15 and somewhat west (left) of targets A-1 and A-2 as evidenced by the polarity of the profile peaks. Another interesting point about the profiles is that the EM-61 gate does not detect the presence of target A-6 (flattened pop can). The target's presence is very clearly indicated by the earlier ("H_z_Mid") gate and the very early H_x gate.

Compiling horizontal components into maps requires additional data processing for two primary reasons. Firstly, the direction of cart travel alternates between adjacent lines. In the simplest case, this alternates the polarity of the measured ***anomalous*** horizontal response between adjacent lines. Horizontal components must therefore be rotated into a common coordinate system. But instrument background is not affected by cart azimuth and consequently its sign does not change with a reversal in direction. Therefore, before horizontal component data can be compiled into map form, background must be removed. Otherwise, the rotation will cause the background level to alternate between lines and thus produce an alternating step pattern. Good background removal is especially important at early times where the instrument-response background is quite high. In Figure 9, we have plotted the horizontal components for 3 adjacent profiles centered over Column D at Blossom Point. These profiles show the 3 vector components after background removal and component rotation. We have plotted the composite of channels 12-21 (21.7-213.3 μs). This figure illustrates that our processing can adequately remove the background and that the rotation and correction for spatial offsets has been properly applied. We have rotated the horizontal components into a geographic coordinate system in which the positive *y*-axis lies to the north and positive *x* is to the east. In this coordinate system, the survey lines are parallel to the *y*-axis. Note that our processing introduces the correct polarities for all anomalies along the 3 lines even though the centerline data were acquired in the opposite direction from the two adjacent lines (the center line 1000210 was acquired going south). Now the horizontal anomaly component along line (H_y) is bipolar with negatives to the south and positives to the north (Figure 10a). The transverse anomalies (H_x) exhibit the expected bipolar behavior, negative on the west and positive on east (Figure 10b).

We can generate an interesting map by computing the total horizontal field magnitude. By construction the parameter is rotationally invariant and non-negative, meaning that it can be used to quickly generate a map without removing background or rotating vector components. Thus it is a map image that can be constructed quickly in the field, similar to vertical intensity maps. A map of total horizontal field intensity is shown in Figure 10c. This map was made using our *very early time* composite gate (1-10 = 0 – 15.6μs). During early times, the horizontal fields have a

high SNR and a relatively low background. This early time horizontal component should be more responsive to small highly conductive objects than the later standard gate. If the targets are low-mass objects that lie near the surface (e.g., mine detonators) the total horizontal field response may be extremely useful. We need to study the use of the very early time horizontal components in test ranges with smaller more conductive targets (a synthetic mine field perhaps).

Figure 2 is the *early time* (channels 10-16, 15-40µs) vertical intensity map that we have used to automatically pick targets. The background of the vertical component at *very early time* is so high that we really need to look farther out in time in order to make an interesting map. But it should be abundantly clear by comparing Figures 2 and 10c (total horizontal field intensity) that horizontal fields measured at early times can be used effectively as a tool for simple detection. We have not had sufficient time to critically evaluate the various measures of the horizontal field strength. Clearly, however, the total horizontal field at *very early times* (Figure 10c) appears qualitatively to be on a par with the *early time* "standard map" (Figure 2) that we used for target detection.

One possible application of the horizontal field intensity may be in UXO detection in magnetic soils and rock such as those found in Kaho'olawe, Hawaii. There is no horizontal field component at the center of a horizontal loop transmitter over a 1-D earth. Therefore, to the extent that geologic background is relatively uniform over lateral distances of a few meters, background geologic effects couple only into the vertical-component receiver antenna   The horizontal components should be relatively free of these magnetic background effects and therefore should have a lower "geologic noise" to signal ratio.
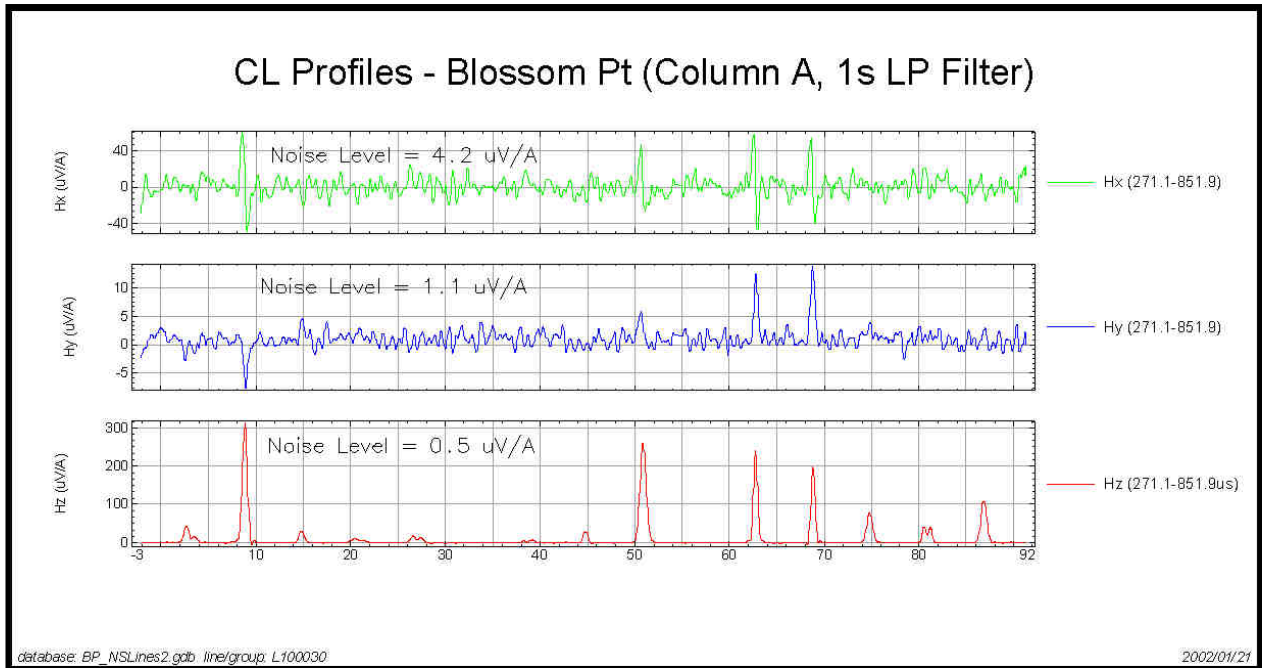
.

Figure 7: Centerline profile over Column A showing vector components after low-pass filtering. Noise levels have been reduced by a factor of 3 over those indicated in Figure 6.
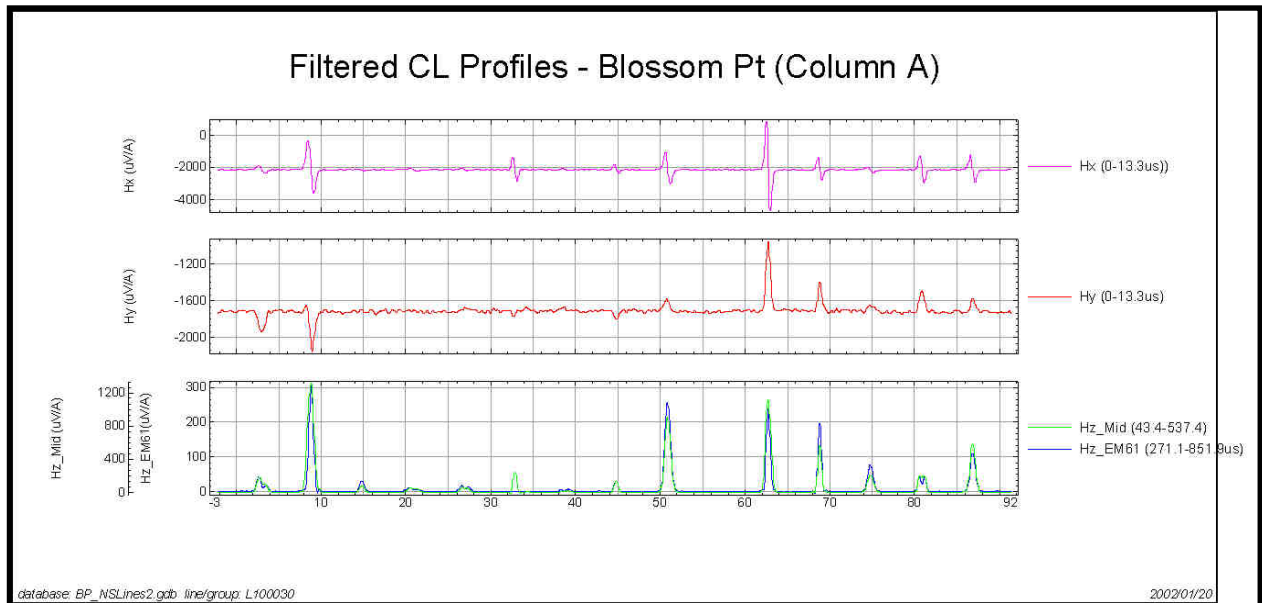

Figure 8: Centerline profile showing horizontal field components (top 2 profiles) at very early time. The bottom profiles represent the vertical field at later time gates.
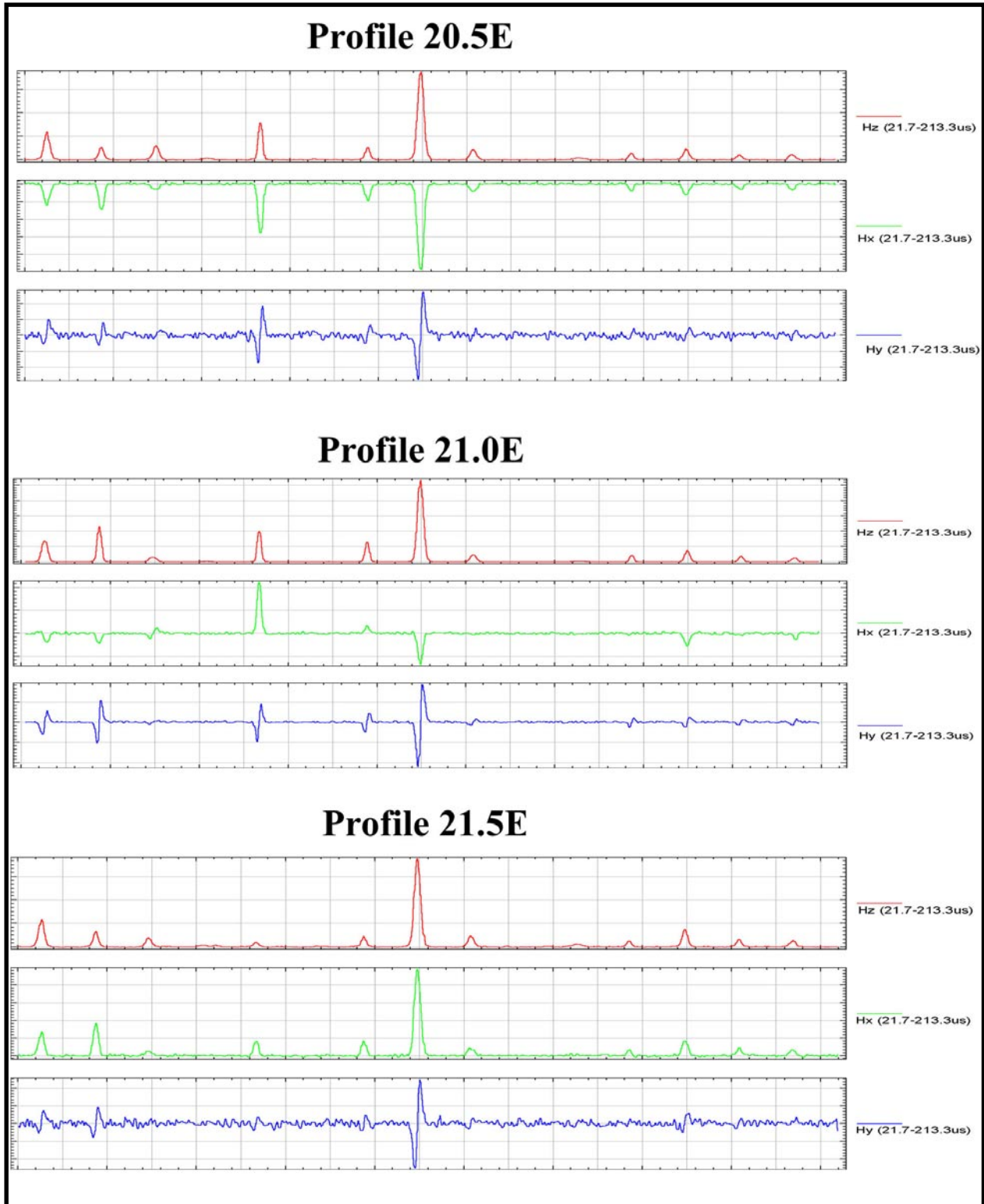
Figure 9: Orthogonal component profiles over 3 adjacent lines centered on Column D at Blossom Point. The profiles illustrate correct background removal and rotation.
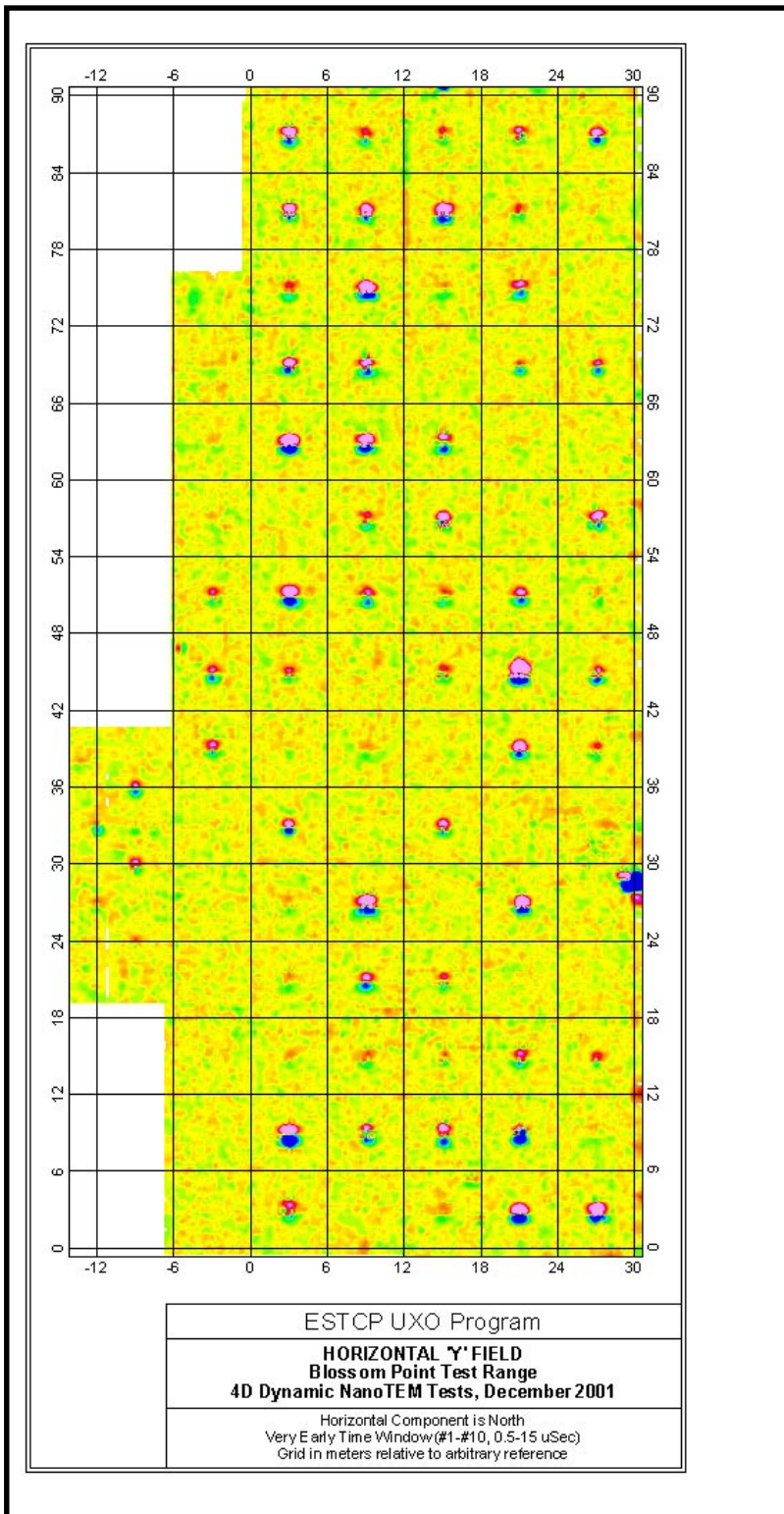
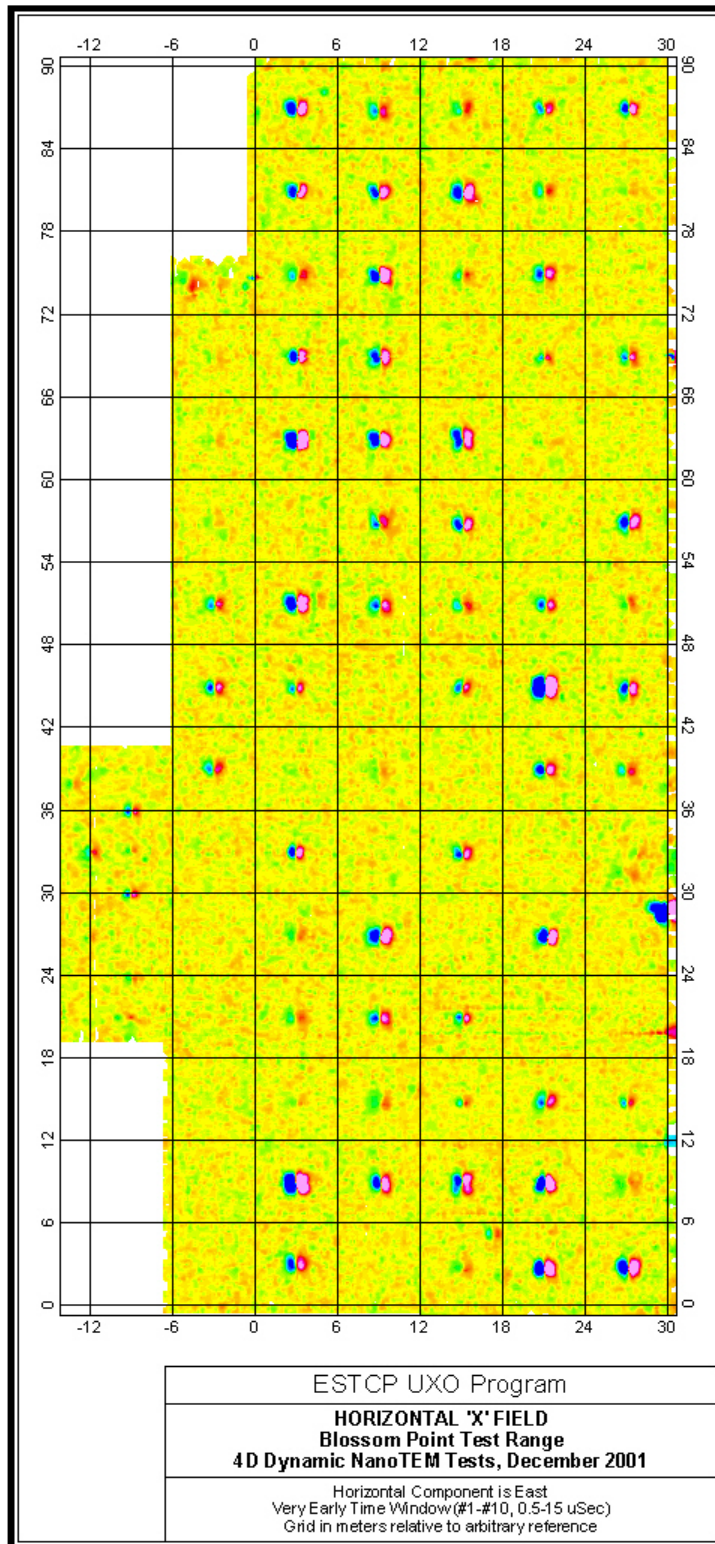**Figure 10a: Compiled map showing the early time anomalous H_y component.**

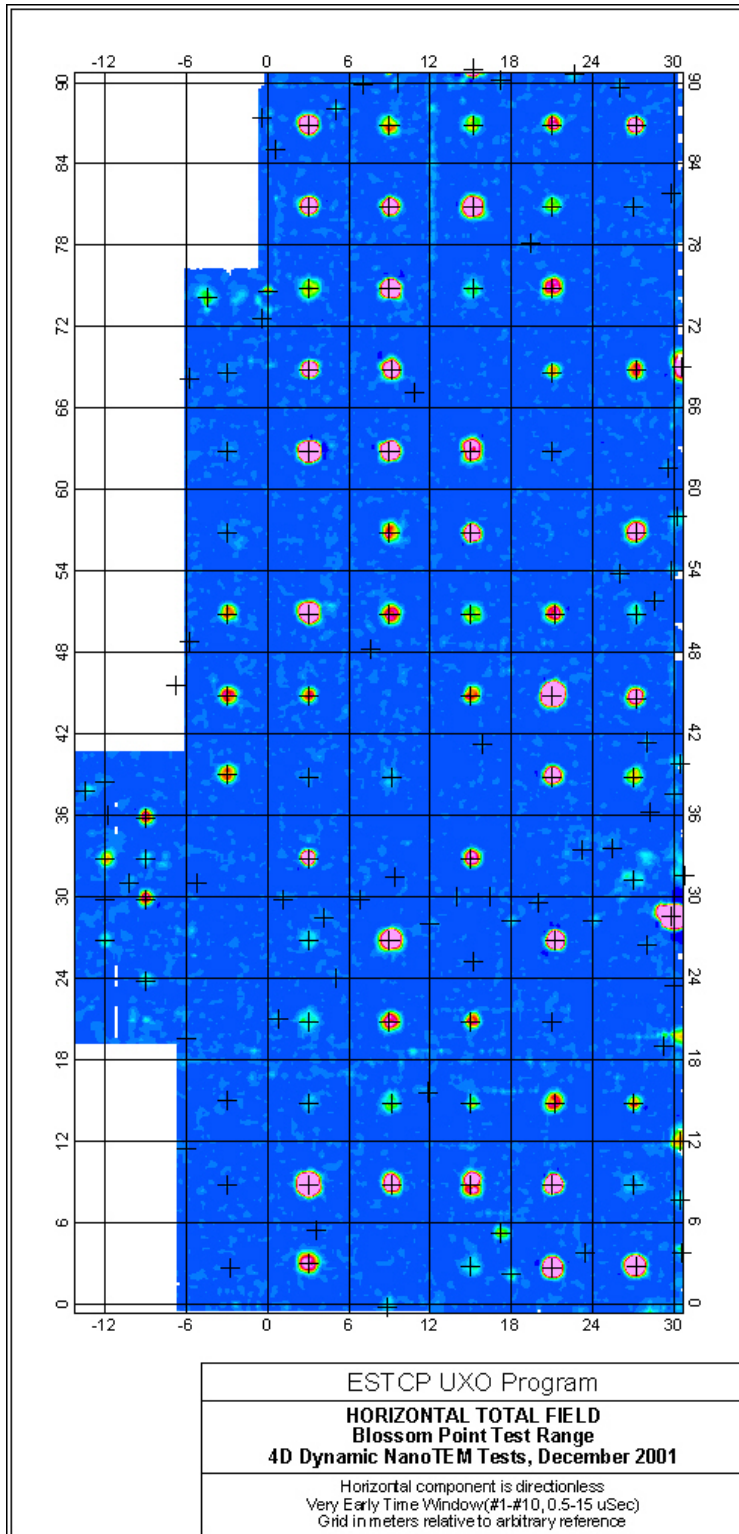**Figure 10b: Compiled map showing the early time anomalous H$_x$ component.**

Figure 10c: Horizontal total field map – very early time

STATIC MEASUREMENTS AND PARAMETERIZATION

We brought a second antenna array and NT-32[II] to Blossom Point for the purpose of acquiring some precision transient data at static points in the vicinity of a target. With this equipment, we made static measurements selected targets. Although we completed static measurements on "9-spot" grids (1/2-m 3x3 grid) over all 14 targets in rows 13, 14, and 15 (one cell uninhabited), not all of the data sets are satisfactory due to problems with our second receiver. Figure 11 is a photograph of the static measurement setup we used at Blossom Point. We centered a rubber mat (station template) containing a 3x3 matrix of "spots" at ½ -m intervals over a point 25cm north of the target location peg and oriented the grid N-S and E-W.[9] The receiver was started while the antenna array was located off of the target presumably measuring background. This allows the instrument to properly set the gain for each channel. Once recording, the antenna array was located at each of the 9 spots of the station

Figure 11: **Test setup for static data acquisition mode (SAM).**

template for approximately 25-30 seconds. A complete set of 13 static measurements (i.e. 2x background + 9 spots + repeat of center location) can be completed in 10 minutes including setup time between target locations.

Raw data are reduced in Geosoft Oasis Montaj. Each target site is recorded into a separate data file. These data are read into Oasis where they are separated into lines (1 line per antenna location). Each line is "stacked" into a single average transient. Residual transients are produced by subtracting the background transient. An example of the resulting 9 stacked residual transients over target A-13 (BDU-33 buried nose down at 75cm) is shown in Figure 12.

In the Figure 12, each set of transients (H_u-NS; H_v-WE; H_w-vertical) is shown in its correct spatial relationship to the target. The center plot represents measurement from the (0,0) spot location that is presumed to be directly over the target. The transients show the correct polarities. There is clearly coherent noise that has been stacked into the transients and is picked up most prominently in the "u" channel (pointed north in this case). The noise level obviously changes with time. The order of measurement of these "spots" proceeds from the center to upper left thence clockwise around the outside ending with a repeat at the center position. The coherent noise spike so clearly evident in the center-right plot increases for a few minutes and then decreases back to "ambient" levels. From the polarities of the horizontal transients we can see that the target lies a bit northeast of the center position.

---

[9] Herb Nelson indicated that the target location pegs were positioned 25cm south of the actual target location.
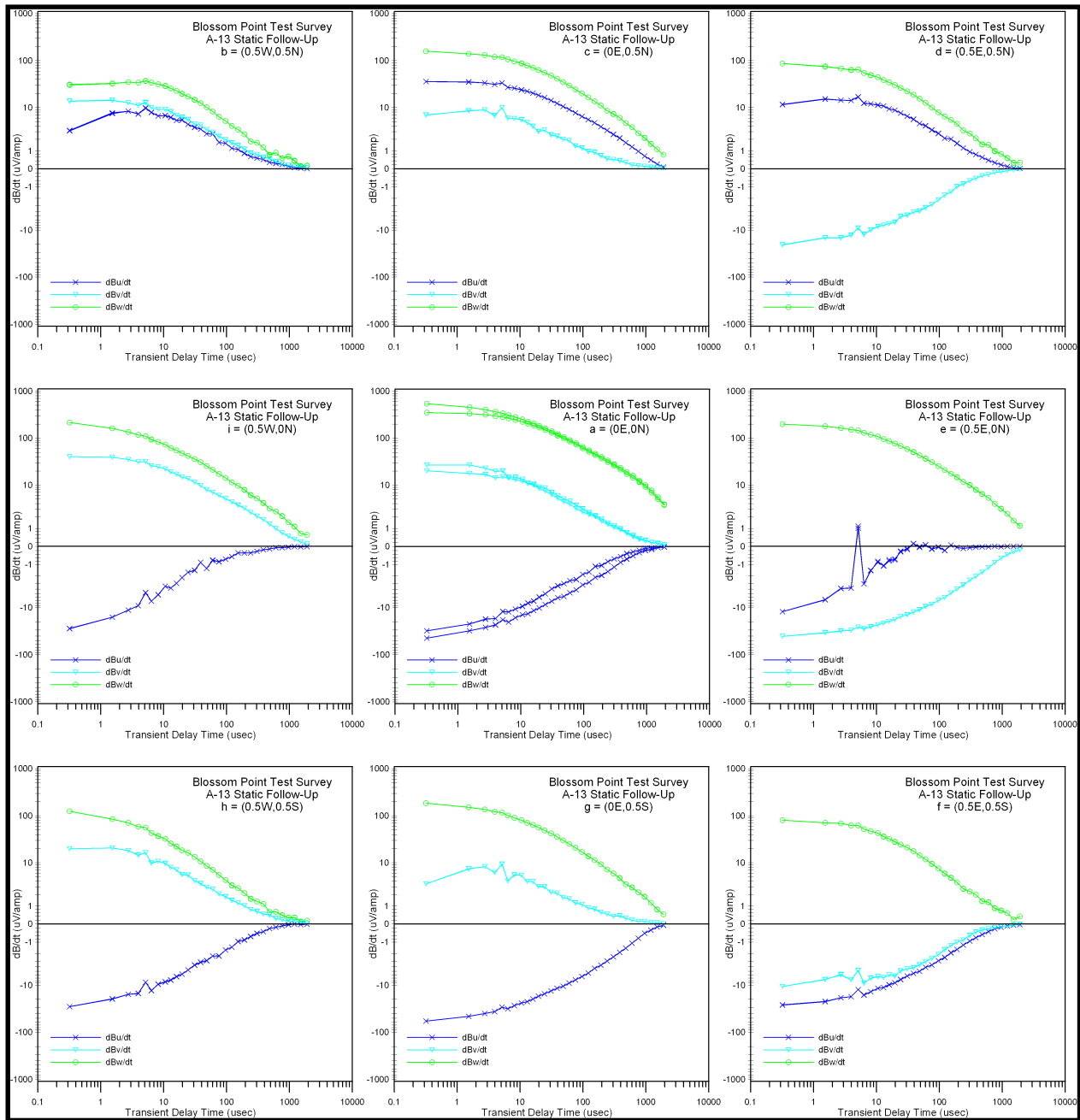
Figure 12: A "9-Spot" of residual 3-Component transients centered over target A-13 at Blossom Point.

The residual transients shown in Figure 12 are the raw data for a target modeling or parameterization program designed to more precisely locate the target, determine if possible its attitude, and parameterize the polarizability tensor. This program (*DNTDipole)* is still under development and this is the first time we have had high quality field data for testing it. The model is a point dipole with an anisotropic polarizability. The UXO community has more or less universally adopted this model. Our model with minor differences has been inspired by the published work of Barrow and Nelson [4], Bell and others [5] , and Pasion and Oldenburg [6]. Other details about the procedures are contained in a paper by MacInnes and others [7] that will be presented in February at the SAGEEP 2002 conference in Las Vegas.

30

Our inversion program is a two-step process. In the first step, we remove the spatial effects caused by taking measurements at any number of field points located in the vicinity of the target. In doing so, we compute an optimal position and a target attitude (i.e., heading, pitch, and roll angles). In addition, the procedure provides us with an estimate of the time derivatives of the three polarizability transients that define the time derivative of the polarizability tensor expressed in its principal axis coordinate system.
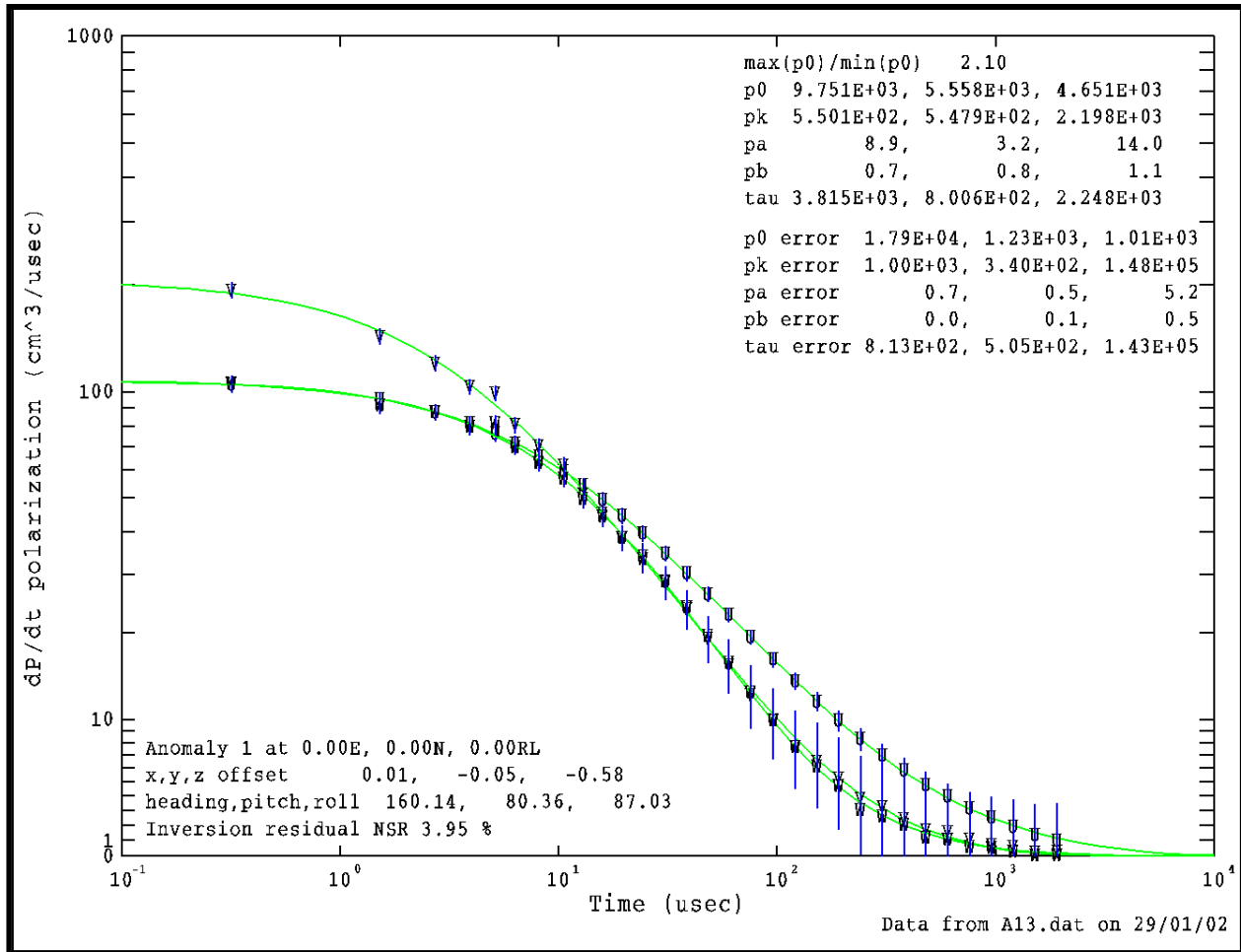

Figure 13: Summary plot containing results of inverting 3-component "9-spot" data obtained over target A-13 at Blossom Point.

In the second step of the inversion process, the three principal polarizability transients are parameterized using the Pasion-Oldenberg model [6] as an expression of their curve shape. Figure 13 presents a summary of this inversion process as applied to 3-component "9-Spot" data shown in Figure 12. NSR[10] residual error (3.95%) is relatively low, indicating a good fit to observed data. The results of the spatial inversion predict a target at a depth of 58 cm below the center of our antenna array. The heading, pitch and roll angles are consistent with the known attitude of the target (vertical).

---

[10] NSR is "Noise to Signal Ratio" and is computed as the ratio of the mean square error between the observed and predicted data to the mean square signal expressed as a percent.

The parameterization of the polarization curves is shown in the upper right hand side of the summary plot in Figure 13. Five parameters are derived for each curve. These parameters are defined below:

$$p_0 = \int_0^\infty \frac{dP}{dt} dt; \text{Inductive limit polarizability} \qquad (1.1)$$

$$\frac{dP}{dt} = p_k \left(t + p_a \right)^{-p_b} e^{-\left(\frac{t}{\tau}\right)}; \text{Pasion/Oldenburg transient model} \qquad (1.2)$$

The ratio of maximum to minimum inductive limit polarizability parameter is somewhat like the "β ratio" used in similar models discussed in literature cited previously. Thus, the model results indicate an elongated target, consistent with the shape of the BDU-33.

Furthermore, the parameter p_0 is an indicator of target size. For a conductive permeable sphere, $p_0 = 2\pi a^3$ (where a is the sphere radius) a value equal to 3/2 times the volume of the sphere. Our parameterization suggests a value of about 5,000 cm³ for p_0(max). This value is consistent with values we have measured in air for large targets such as a 105mm howitzer projectile.
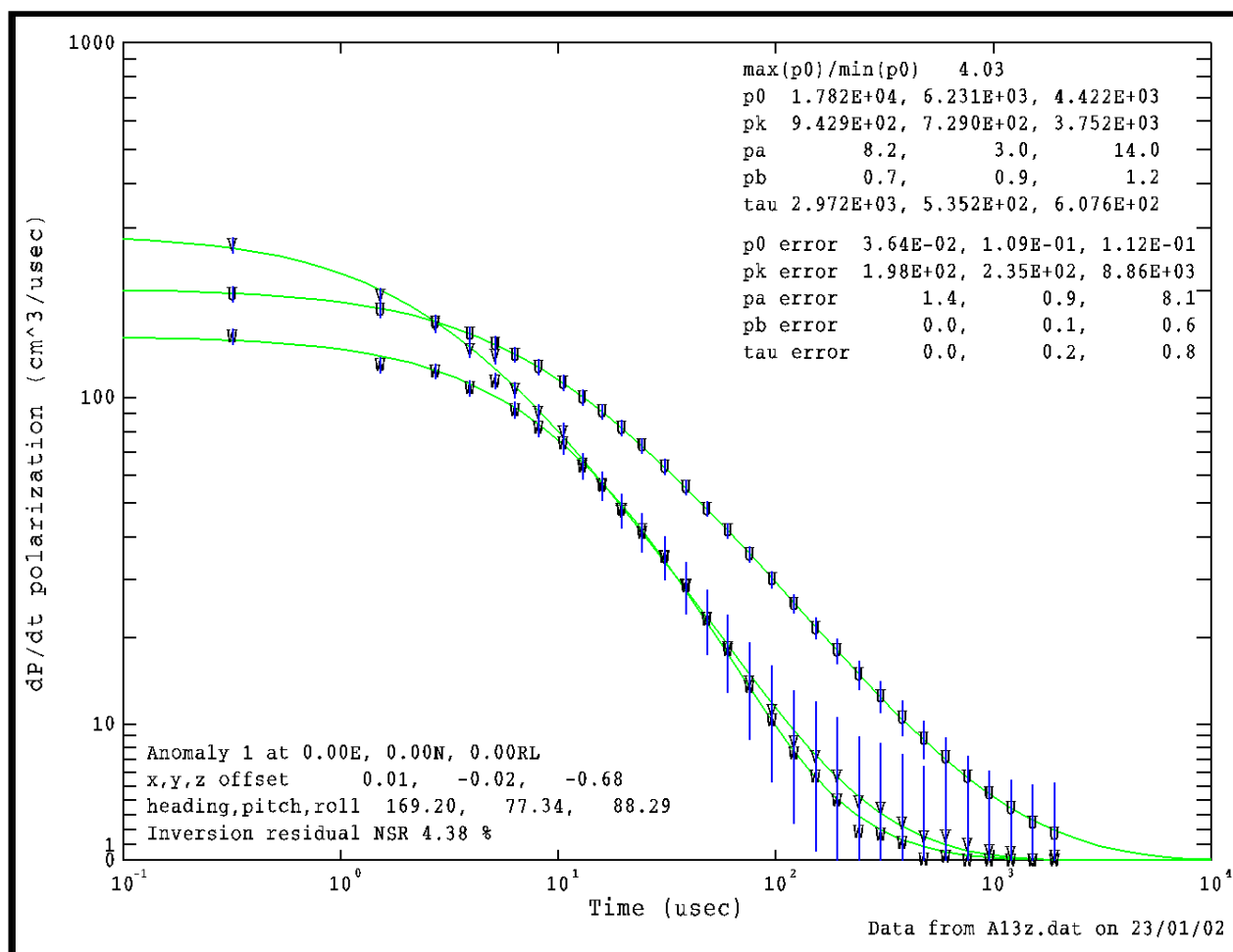

Figure 14: Inversion results from *DNTDipole* using vertical response only from the 9-spot over target A-13.

32

We have observed in this report that the anisotropy of the target response gets more pronounced at later times. This observation is confirmed by examples such as that shown in Figure 5. The early-time response may include additional information about target shape, but we do not yet have enough experience to interpret the meaning of the early-time crossovers seen in Figure 5 to predict the target depth and its attitude.

We also inverted the A-13 9-spot using just vertical component data. Those results are summarized in Figure 14. As with the 3-component analysis in Figure 13, the results of the analysis of the single (vertical) component data also consistent with known target properties, with even a stronger prediction of target elongation (max(p0)/min(p0)=4).

We have completed testing of our model using the "9-spots" we collected at Blossom Point. We summarize those results in Table 5 (3-component inversions) and Table 6 (z-component inversions). Generally speaking, the model works well in refining the target position. The standard deviations of the error between the true target depth and actual target depth are 14cm and 21 cm respectively for the two inversion modes. These results would be even better were we to eliminate two of the 9-spots (D-15b and E-14). The results tabulated in Tables 5 and 6 represent only a subset of the parameters that we derive from this process of parameterization (we have omitted the 4 Pasion-Oldenburg curve parameters). We have not had time to evaluate or correlate these properties with the physical characteristics of each target. We can see an obvious correlation between the ratio of the maximum to minimum polarizabilities (p0_mx/mn) and target aspect. This comes as no surprise since this parameter is equivalent to the β ratio parameter currently being used by authors previously cited. The magnitude of the 3 polarizability parameters (p_i) is related to the physical volume of target. And the inversion results indicate that target E-14 (a 3"x24" steel cylinder) is the largest target evaluated. Inversion results using the Z-component data alone do a better job of determining target attitude. We have not had sufficient time to experiment with variations in the application of our inversion code to be able to offer an explanation for this result. The value of the horizontal component data to quantitative target characterization has not been demonstrated.

This inversion model will be applied using data acquired in the dynamic acquisition mode. We still have much to learn about the meaning of the parameters *vis-à-vis* target classification. The Blossom Point data set provides us with a rich variety of targets to experiment with.

Table 5: Summary of 3-component full waveform inversion results for 9-Spot data acquired at Blossom Point.

	Targets					3-Component Modeling Results								
TRG	Description	Depth (m)	hdg (deg)	Pitch	Aspect Ratio	$|z\_mod|$ (m)	$|zmod|-|z|$ (m)	hdg (deg)	Pitch (deg)	roll	p0_mx/mn	p0_1 (cm³)	p0_2 (cm³)	p0_3 (cm³)
A13	BDU-33 25 lb bomb	0.75	0	90	8	0.58	-0.17	160	80.4	87	2.1	9.75E+03	5.56E+03	4.65E+03
A14	4"x4"x0.25" steel plate	0.05	45	0	16	0.27	0.22	-44.7	-29.0	2.3	15.3	3.83E+03	1.49E+03	2.51E+02
A15	16 lb shotput	0.25	0	0	1	0.32	0.07	-8.5	54.5	0.6	2.3	1.66E+03	2.74E+03	3.88E+03
B13	3"x6" steel cylinder	0.10	0	90	2	0.13	0.03	73.4	42.5	-4.4	1.5	1.68E+03	1.17E+03	1.13E+03
B14	MK 23, 2" x 8" cylinder	0.25	0	90	4	0.31	0.06	-26.1	64.4	3.6	9.1	3.67E+03	4.61E+02	4.02E+02
B15	3"x12"x0.25" steel plate	0.25	0	0	4	0.39	0.14	-4.5	-2.3	23.4	7.2	6.85E+03	1.53E+03	9.52E+02
C13	3"x12" steel cylinder	0.50	0	0	4	0.45	-0.05	75.8	-39.0	3.5	1.8	2.71E+03	1.77E+03	3.18E+03
C14	8"x8"x0.25" steel plate	0.20	45	0	32	0.47	0.27	-70.7	33.5	5.7	2.5	1.15E+04	1.68E+04	6.61E+03
C15	1.5"x6" steel cylinder	0.25	0	90	4	0.29	0.04	-0.6	-1.2	47.7	4.8	1.59E+03	3.31E+02	4.39E+02
D13	81 mm mortar	0.35	0	0	6	0.23	-0.12	-87.2	0.9	88.8	1.6	1.36E+03	1.07E+03	8.55E+02
D14b	1.5"x12" steel cylinder	0.35	0	90	8	0.38	0.03	-71.7	-64.3	79.3	20.9	6.74E+02	5.26E+03	2.52E+02
D14a	1.5"x12" steel cylinder	0.35	0	90	8	0.44	0.09	86.4	-27.1	36.9	8.5	7.91E+03	9.27E+02	1.92E+03
D15a	1.5"x3" steel cylinder	0.05	0	0	2	0.08	0.03	-15.6	0.5	-9.4	2.6	2.26E+02	1.12E+02	8.55E+01
D15b	1.5"x3" steel cylinder	0.05	0	0	2	0.21	0.16	-17.6	-23.0	-3.1	6.6	8.94E+02	4.93E+02	1.36E+02
E14	3"x24" steel cylinder	0.75	0	0	8	1.06	0.31	8.8	-5.4	1.2	2.2	4.63E+04	2.70E+04	2.10E+04
E15	1.5"x6"x0.25" steel plate	0.08	0	90	24	0.05	-0.03	82.8	-80.5	71.2	7.3	3.70E+02	1.04E+02	5.07E+01
	standard deviations						0.14							

Table 6: Summary of Z-component full waveform inversion results for 9-Spot data acquired at Blossom Point.

TRG	Targets Description	Depth (m)	hdg (deg)	Pitch	Aspect Ratio	|z_mod|	|zmod|-|z|	hdg (deg)	pitch (deg)	roll	p0_mx/mn	p0_1	p0_2	p0_3
A13	BDU-33 25 lb bomb	0.75	0	90	8	0.71	-0.04	82.0	79.9	87.6	5.10	2.15E+04	5.83E+03	4.21E+03
A14	4"x4"x0.25" steel plate	0.05	45	0	16	0.15	0.10	-63.3	-0.7	80.8	5.41	1.16E+03	2.14E+02	1.13E+03
A15	16 lb shotput	0.25	0	0	1	0.34	0.09	-63.0	20.0	42.2	1.43	3.98E+03	2.87E+03	4.11E+03
B13	3"x6" steel cylinder	0.10	0	90	2	0.17	0.07	-87.5	-74.7	84.1	1.26	1.87E+03	1.71E+03	1.48E+03
B14	MK 23, 2" x 8" cylinder	0.25	0	90	4	0.27	0.02	30.6	85.4	-36.2	6.21	2.48E+03	4.00E+02	6.26E+02
B15	3"x12"x0.25" steel plate	0.25	0	0	4	0.29	0.04	-88.5	25.5	13.0	25.89	1.37E+03	3.85E+03	1.49E+02
C13	3"x12" steel cylinder	0.50	0	0	4	0.64	0.14	65.2	-79.7	75.1	5.26	1.14E+04	2.49E+03	2.17E+03
C14	8"x8"x0.25" steel plate	0.20	45	0	32	0.24	0.04	-84.7	-3.3	6.5	5.41	4.38E+03	4.73E+03	8.74E+02
C15	1.5"x6" steel cylinder	0.25	0	90	4	0.20	-0.05	-1.7	12.8	1.2	6.98	9.57E+02	3.08E+02	1.37E+02
D13	81 mm mortar	0.35	0	0	6	0.16	-0.19	-82.9	20.6	14.9	2.09	1.08E+03	6.21E+02	5.16E+02
D14b	1.5"x12" steel cylinder	0.35	0	90	8	0.42	0.07	-82.4	84.2	-100.2	5.95	3.47E+03	6.33E+02	5.83E+02
D14a	1.5"x12" steel cylinder	0.35	0	90	8	0.50	0.15	58.1	-83.6	20.5	2.10	6.67E+03	3.17E+03	3.26E+03
D15a	1.5"x3" steel cylinder	0.05	0	0	2	0.18	0.13	-19.1	-8.0	-53.9	3.21	4.63E+02	2.06E+02	1.44E+02
D15b	1.5"x3" steel cylinder	0.05	0	0	2	0.71	0.66	-2.1	-52.3	87.2	2.31	1.11E+04	7.78E+03	4.82E+03
E14	3"x24" steel cylinder	0.75	0	0	8	1.31	0.56	7.1	-4.1	89.3	2.46	1.05E+05	6.31E+04	4.26E+04
E15	1.5"x6"x0.25" steel plate	0.08	0	90	24	0.08	0.00	-80.1	81.5	101.2	7.63	4.45E+02	9.00E+01	5.83E+01
	standard deviations						0.21							

CONCLUSIONS

We have successfully concluded our demonstration at Blossom Point. Our instruments, our software, and our analysis have provided data and information not previously available from Blossom Point. We believe our work is worthy of continuation in the ESTCP Program. We have just now reached the point where we can make more substantial contributions by collecting and assessing data.

We have submitted with this report a unique set of 4-D fast TEM data (i.e., *Documented Data Set*) that will help others to begin work with "4-D TEM". And we have provided in this report a comparison of 3 transient electromagnetic systems being applied to UXO detection and classification.

There is no question in our minds that our system and data displays offer "Added Value" compared to conventional equipment. We have demonstrated that target differentiation is possible and that 'early times' are necessary to provide this differentiation.

For small targets, the early time capabilities of the DNT system gives us the ability to detect targets significantly smaller than those detectable by conventional equipment, principally the EM-61. For larger targets, we were disappointed that our system did not provide expanded range compared to conventional equipment. If the sole function of a TEM survey is only to detect and map larger targets, then we cannot claim that we have a superior system. However, we can claim that our system offers "equal value." Overall, the NanoTEM system has demonstrated that it has somewhat better sensitivity than the EM-63 as it was deployed at Blossom Point. The comparison of the NanoTEM system with the EM-61 demonstrates that at the speed at which we surveyed (~30 m/min), the NanoTEM system has a sensitivity for large objects that is comparable to that of the man-portable MTADS EM-61.

Specifically, we believe that we add value to the ESTCP Program and have demonstrated it in the following ways:

1. Early times are very useful in detecting small conductive objects. Target A-6 and the little survey tape swivels are examples of targets that generate little or no response from an EM-61 or EM-63. EM-6? transmitters are too slow and the time delay to the first gate is too long to detect the quickly decaying transients generated by small targets. With a multiple time gate system, we are able to adjust the detection time gate during our post-processing to optimize detection of a specific range of target sizes. Small targets generate shorter transient signals and are best detected with early-time data. Detecting larger targets is better accomplished using the response at later times.

2. Horizontal component measurements respond better at early times because the instrument-response and geologic background is significantly smaller. To a first approximation, horizontal components are null-coupled with the transmitter. Moreover, our results demonstrate that early time measurements are necessary to observe the horizontal components because there are higher EMI noise levels in the horizontal components and, except for the largest targets, the amplitude of these anomalies is too small to be useful at later times. That said, however, we have demonstrated that we are able to observe the horizontal fields with adequate sensitivity. We have examples in other applications of this 4-D TEM technology where early-time horizontal components are the only indication of a

target. However, at Blossom Point all detectable targets are visible in both horizontal and vertical component data.

3. Horizontal components are able to determine lateral target offset when the antenna cart has not passed directly over the target. It is obvious from these data that the transverse horizontal component is a sensitive indicator of lateral offset. Inversion of data to recover target properties is improved by including horizontal components, since there is better control of the target's location with respect to the measurement profile centerline. Measuring horizontal components may also permit the lane spacing to be widened for surveys where simple detection is the objective.

4. The DNT system, with its ability to record 31 time gates at the rate of 32 samples/sec, provides unprecedented anomaly resolution. This sample density can be exploited in two ways. It can help to improve productivity by allowing the antenna array to be moved faster. Additionally, it facilitates significant noise reduction through low-pass filtering. That filtering can be adjusted during the post-survey data processing to optimize performance for particular survey speeds and targets. As post-processing filters are not limited by real-time data acquisition constraints, they can use computationally intensive non-linear algorithms to improve results in the presence of non-gaussian noise.

5. The 4D-TEM system is flexible and can be reconfigured to optimize survey conditions. Reacquisition follow-up measurements can be made with a different cart configuration. Or, as was demonstrated in the Blossom Point survey, precision static measurements can be acquired with the same instrument and antenna array. Inversion to recover target properties benefits from data sets collected using more than one system configuration. Combining data sets with multiple loop elevations is equivalent to measuring magnetic field gradients and puts strong constraints on estimates of target depth. We expect that inversion using combined dynamic data (with loops elevated 26 cm above ground) and static data (with the loop elevated 6 cm above ground) will produce even better modeling results.

6. The time-decay characteristics of the signal are dependent on the target. But we have shown in this survey that, with early times and 31 time-window recording, it is possible to make some distinctions between targets with simple and easily implemented techniques. If this work is continued, we look forward to correlating simple empirical parameters to target characteristics as well as correlating the complex modeling/inversion parameters to target characteristics.

7. We have demonstrated the ability to perform inversions using the 4 dimensions of our data collection system. The results from these inversions are very encouraging and demonstrate that useful parametric information can be derived from these inversions. But we need to systematically apply this interpretation tool to other targets and to compile the results in order to demonstrate how target identification and classification is improved.

REFERENCES

1. Nelson, H.H., J.R. McDonald, and Richard Robertson, *Design and Construction of the NRL Baseline Ordnance Classification Test Site at Blossom Point*. 2000, Naval Research Laboratory: Washington, DC. p. 13.

2. Snyder, D.D., *UXO Characterization with a Fast 4-D TEM System: Blossom Point Classification Test Site*. 2001, Zonge Engineering and Research Organization: Tucson. p. 21.

3. Carlson, N.R., and Kenneth L. Zonge. *Early-time, Multi-Component Mobile TEM for Deep Metal Detection*. in *SAGEEP 2002*. 2002. Las Vegas, NV: EEGS.

4. Barrow, B.a.H.H.N., *Model-based characterization of electromagnetic signatures obtained with the MTAD electromagnetic array*. IEEE Trans. on Geos. & Remote Sensing, 2001. **6**: p. 1279-1285.

5. Bell, T.H., B. Barrow, and J.T. Miller, *Subsurface discrimination using electromagnetic induction sensors*. IEEE Trans. on Geos. & Remote Sensing, 2001. **6**: p. 1286-1293.

6. Pasion, L.R.a.D.W.O. *Locating and determining dimensionality of UXOs using time domain induction*. in *SAGEEP 1999*. 1999. Oakland, CA: EEGS.

7. MacInnes, S.C., Donald D. Snyder, David C. George, and Kenneth L. Zonge. *Model-Based UXO Classification Based on Static 3-Component TEM Measurements*. in *SAGEEP 2002*. 2002. Las Vegas: EEGS.

Attachment A

DOCUMENTED DATA SET
DATA FROM BLOSSOM POINT TEST RANGE
DECEMBER 11 – 14, 2001

Zonge Engineering & Research Organization
3322 East Fort Lowell Road
Tucson, AZ 85716
http://www.Zonge.com
(520) 327-5501

GENERAL DESCRIPTION

The data are contained in three files:

- North-South lines, file BPNorthSouth.csv. This file contains data for lines running north-south at 0.5 meter line spacing.

- East-West lines, file BPEastWest.csv. This file contains data for lines running east-west at 1.0 meter line spacing.

- Calibration lines, file BPCalibrations.csv. This file contains data for calibration lines. These calibrations were run and repeated over a fixed target (a steel ball) at a fixed location.

GPS data were collected with a Leica model SR530 Real Time Kinematic (RTK) GPS system. The GPS data were reduced with Leica 'SkiPro' software.

Electromagnetic data were collected with the Zonge Engineering GDP-32^{II} receiver running a newly developed software package: *DyNanoTem*. These data were collected from each of three orthogonal receiving loops sampled at approximately 1.2 μs (830.124 kHz) following the turnoff of the transmitted signal. 2048 samples are collected for each receiver channel and reduced by simple averaging to 31 'time windows.' The transmitter waveform (one positive pulse and one negative pulse) is repeated at a rate of 32 Hz and individual transients are recorded. Each recorded transient is the sum of one positive and one negative transient. Thus the data in the files are one transient of 31 points for each of the three received signals at a rate of 32 transients per second.

Clock time was independently recorded in both the GPS system and the GDP-32^{II} system. These clock times were used during data reduction to align TEM data with correct GPS coordinates.

For calibration, the receiving system was pushed forward over the calibration ball and then pulled backward over the ball. The TEM anomalies observed from the forward and reverse data were used to adjust time differences between the GPS and GDP-32^{II} clocks.

The data presented in these data files is unedited raw data with the following exceptions:

- Ancillary, 'junk' data collected when the cart was moved outside of the grid or away from the calibration ball has been discarded. This includes data collected while the cart was being turned around at the end of a line to begin another, and data that was collected when the system 'wandered' away from a meaningful line. The effect of discarding this data is to 'clean up' the data set.

- The data have been manually separated into 'lines.' The raw data were continuously collected. Line numbers have been manually assigned and do not exactly represent any 'average' line coordinate.

- The GPS data were merged with the TEM data. The data set includes the coordinates of the GPS antenna at the time of a TEM measurement, and it includes the coordinates of the TEM loops at the same time. The coordinates of the TEM loops are computed from the GPS antenna coordinates by knowing the orientation and geometry of the cart.

Coordinate Reference

All of the data in this survey were collected in absolute UTM coordinates (UTM Zone 18, NAD83). The coordinate data contained in the files have been localized to the following local origin of coordinates[11]:

     X0: 316259.98 meters east
     Y0: 4254164.95 meters north

Loop and Cart Geometry

The local coordinate system of the cart is represented as U-V-W coordinates. In this system the U coordinate is aligned positive with the forward direction of the cart, the V coordinate is aligned positive with the left hand direction, and the W coordinate is aligned positive upward. The receiving loops are aligned with the U-V-W axes and are connected with positive polarities accordingly. The heading of the cart is the compass heading of the U axis with north at zero degrees and east at 90 degrees. The cart is assumed to be level, that is no pitch or roll. Dimensions of critical points on the cart (loop centers and GPS antenna) are shown in Figure A1.

The transmitter loop is polygonal in shape with an area of 0.926 m^2 with eight (8) turns. The receiving loops are square and approximately 0.5 meters on a side and contain twelve (12) turns. Precise dimensional measurements together with calculated cross-sectional areas for all loops is provided in Figure A2. The receiving loops were aligned and connected, polarity-wise, as shown in Figure A1.
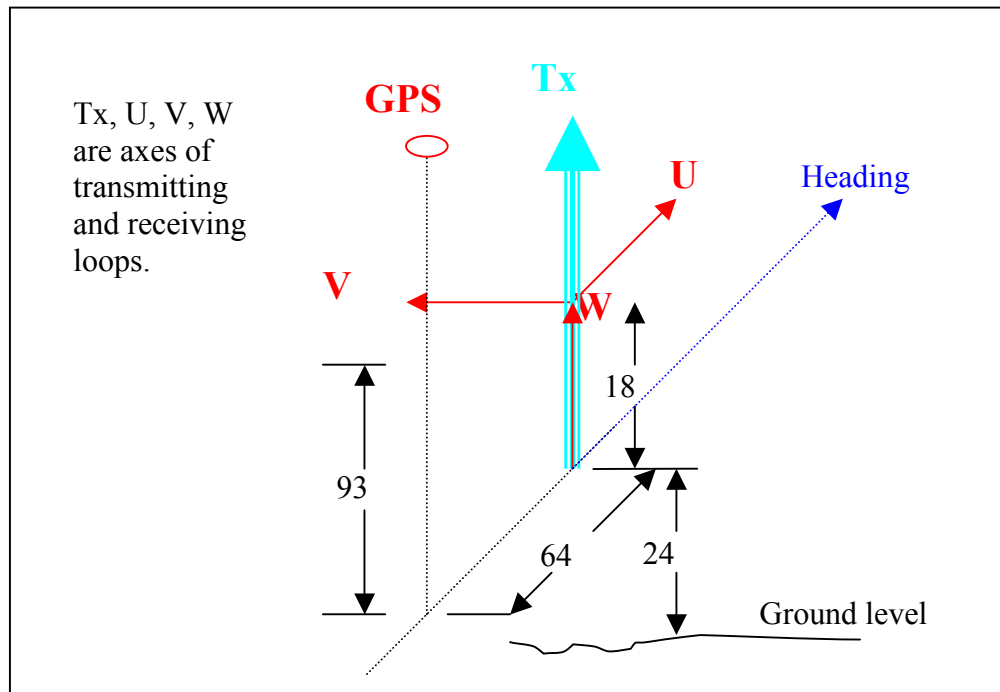

Figure A1: Cart Geometry and Dimensions

---

[11] The local origin of coordinates is 3m west and 2.75 meters south of the plastic stake marking target A-1. It is our understanding from Herb Nelson (NRL) that these stakes are located 25cm south of the actual target location. Thus our origin of coordinates has been placed at the lower left hand corner of the 30m x 100m test area (see Figure 3, Nelson, et. al., 2000).
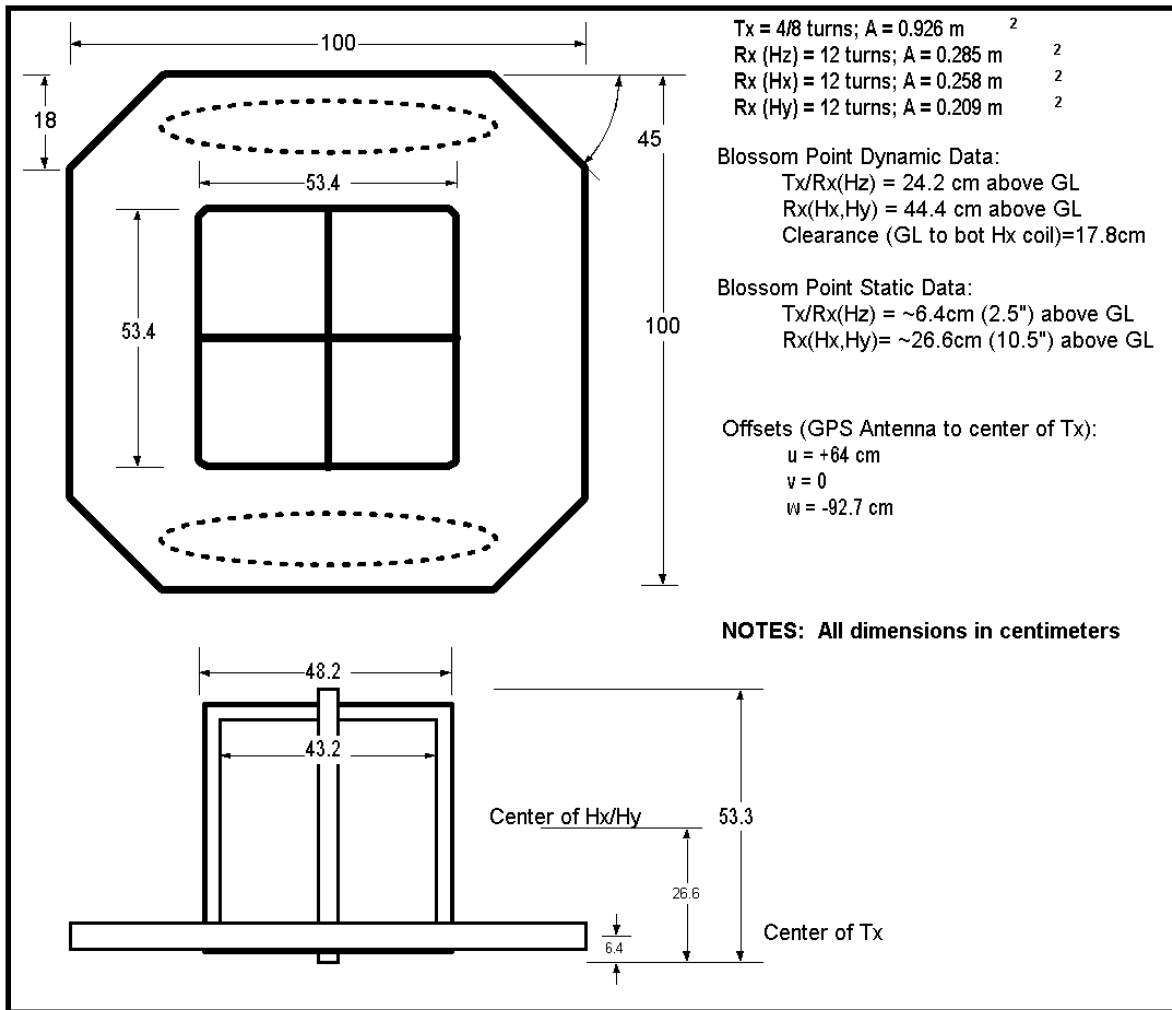
Figure A2: Antenna dimensions for Dynamic NanoTEM system employed at Blossom Point.

Window Times

The beginning time and width of each of the 31 windows are given in Table A1. After the current is turned off, the receiver is 'held off' for a specific number of time intervals (8 in the case of these data) after which the signal is sampled at a rate of 830.124 samples/sec (Δt = 1.20464 μs). The first few time windows consist of a single sample of the received signal. Later windows are the average of the number of samples of the input signal corresponding to each time window as indicated in the Table.

Table A1: Standard Zonge NanoTEM transient window times

Window	32 Hz / 1.2 us Sample Interval			
	Points / Window	Window Center (usec)	Window Width	
			Beg	End
1	1	0.0	0.0	0.0
2	1	1.2	1.2	1.2
3	1	2.4	2.4	2.4
4	1	3.6	3.6	3.6
5	1	4.8	4.8	4.8
6	1	6.0	6.0	6.0
7	2	7.8	7.2	8.4
8	2	10.2	9.6	10.8
9	2	12.6	12.1	13.3
10	3	15.6	14.5	16.9
11	3	19.2	18.1	20.5
12	5	24.0	21.7	26.5
13	6	30.6	27.7	33.7
14	7	38.4	34.9	44.2
15	9	48.0	43.4	53.0
16	11	59.9	45.2	66.3
17	15	75.4	67.5	84.4
18	19	95.8	85.6	107.2
19	23	121.0	108.5	135.0
20	29	152.1	136.2	169.9
21	36	191.0	171.1	213.3
22	47	240.6	214.5	269.9
23	58	303.5	271.1	339.8
24	72	381.4	341.0	426.6
25	92	479.5	427.8	537.4
26	116	604.0	538.6	677.2
27	145	760.2	678.4	851.9
28	184	957.1	853.1	1074.0
29	231	1205.0	1075.0	1352.0
30	289	1517.0	1353.0	1700.0
31	369	1910.0	1701.0	2145.0
Total	1780			.

Detailed Description

The data files are comma separated values (csv) text files. For the discussion herein, a 'line' is taken to be a set of data collected along a survey line. A 'record' is taken to be a single line of text in the csv data file.

The first few records of the data file are descriptive header records that begin with a right slash. The last record of these header records is a record containing labels for the data records to follow.

Following the header records and preceding a set of data records, is a record giving the type of line and its number. This line-number-record precedes each set of multiple data records. In this data, calibration lines are of type 'special' and survey lines are of type 'line.' The line number is alphanumeric but not numeric.

Data records are repeated for all the data in one survey line. Each record contains 102 values described in Table A2.

Table A2: Data file content and format

Time	Clock time that the data point is collected. Format is "hh:mm:ss.ss" where hh is hours after midnight, mm is minutes, and ss.ss is seconds and hundredths of seconds.
TxI	Transmitter current in amps. This current is not accurate because it is not recorded with enough precision. Current decreases on the order of 10% as the transmitter battery discharges.
XGPS, YGPS, ZGPS	Coordinates of the GPS antenna in meters. Data are UTM coordinates translated to a local coordinate system as described above.
X0, Y0, Z0	Coordinates of the center of the transmitter/Hz loop. These coordinates are computed from the cart measurements and Heading0.
Heading0	Compass heading of the line. At Blossom Point, all lines are north-south or east-west. The calibration line was on a heading of 347 degrees.
Trans0[0] – Trans0[30]	31 columns of data for each time window for the 'W' or vertical loop. The data are input voltage * 10, in microvolts; i.e. an input of 5 microvolts is the number 50 in the data file.
Trans1[0] – Trans1[30]	Same as Trans0 but for the 'U' or horizontal-forward loop.
Trans2[0] – Trans2[30]	Same as Trans0 but for the 'V' or horizontal-right-side loop.